Self-consistent conversion of a viscous fluid to particles

Denes Molnar and Zack Wolff

Phys. Rev. C **95**, 024903 — Published 8 February 2017

DOI: 10.1103/PhysRevC.95.024903

Self-consistent conversion of a viscous fluid to particles

Denes Molnar and Zack Wolff
Department of Physics and Astronomy, Purdue University, West Lafayette, IN 47907
(Dated: July 10, 2016)

Comparison of hydrodynamic and "hybrid" hydrodynamics+transport calculations to heavy-ion data inevitably requires the conversion of the fluid to particles. For dissipative fluids the conversion is ambiguous without additional theory input complementing hydrodynamics. We obtain self-consistent shear viscous phase space corrections from linearized Boltzmann transport theory for a gas of hadrons. These corrections depend on the particle species, and incorporating them in Cooper-Frye freezeout affects identified particle observables. For example, with additive quark model cross sections, proton elliptic flow is larger than pion elliptic flow at moderately high p_T in $Au + Au$ collisions at RHIC. This is in contrast to Cooper-Frye freezeout with the commonly used "democratic Grad" ansatz that assumes no species dependence. Various analytic and numerical results are also presented for massless and massive two-component mixtures to better elucidate how species dependence arises. For convenient inclusion in pure hydrodynamic and hybrid calculations, Appendix G contains self-consistent viscous corrections for each species both in tabulated and parameterized form.

I. INTRODUCTION

The most common dynamical framework to interpret data from ultrarelativistic heavy-ion ($A + A$) reactions is relativistic hydrodynamics[1]. Application of hydrodynamics necessitates the conversion of the fluid to particles, which are then either evolved further in a hadronic transport model or assumed to free stream to the detectors. The usual approach to such "particlization" [2] is to do the conversion on a constant temperature or energy density hypersurface in spacetime via the Cooper-Frye formula[3]. While unambiguous for fluids in perfect local thermal equilibrium, i.e., *ideal* fluids, for *dissipative* fluids an infinite class of phase space densities can reproduce the same hydrodynamic fields. This is further exacerbated for mixtures where one can postulate phase space corrections for each particle species almost independently.

In practice these ambiguities are commonly ignored, even in state-of-the-art "hybrid" hydro+transport calculations[4]. For example, shear viscous corrections are simply assumed to follow quadratic momentum dependence with a common coefficient for all species, a procedure one of us termed "democratic Grad" ansatz[5]. This, however, ignores the very microscopic dynamics that keeps the hadron gas near local equilibrium. We apply here instead a self-consistent approach that obtains shear viscous corrections from linearized kinetic theory for a gas of hadrons. This extends earlier studies that considered massless quarks and gluons[6], or hadronic mixture with two species only[5].

Recently there has been a lot of interest in bulk viscous corrections [7–9]. While this work focuses on phase space corrections due to shear only, the technique used here could be extended to the bulk viscous case in a straightforward manner. Shear corrections also affect photon and dileption emission from the quark-gluon plasma in heavy-ion collisions[10].

For simplicity we consider phase space corrections with power-law momentum dependence, most prominently the quadratic Grad form, so that the corrections can be simply represented by numbers (instead of numerically determined functions). This will be remedied in a future publication. General aspects of the approach are presented in Section II, followed by analytic and numerical results for massless and massive two-component mixtures in Sections III and IV, and numerical results on the particle species dependence of differential elliptic flow $v_2(p_T) \equiv \langle \cos 2\phi \rangle_{p_T}$ for a multicomponent hadronic gas in Section V. The approach is also verified against fully nonlinear kinetic theory in Section III B. Technical details are deferred to Appendices A-F. We only highlight here Appendix G, which contains tables and parameterizations of self-consistent species-dependent correction factors to the commonly used "democratic" Cooper-Frye freezeout. These facilitate implementation of our results in hydrodynamic and hybrid calculations.

II. VISCOUS PHASE SPACE CORRECTIONS FROM LINEARIZED TRANSPORT

A. Democratic Grad ansatz

The principle challenge in converting a fluid to particles is that one needs to obtain phase space densities

$$f_i(x,\mathbf{p}) \equiv \frac{dN_i(\mathbf{r},\mathbf{p},t)}{d^3r\,d^3p} \tag{1}$$

for each of the particle species i solely from hydrodynamics fields, namely the energy-momentum tensor $T^{\mu\nu}$ and any conserved charge currents N_c^μ (in heavy-ion physics applications, typically the baryon charge). The conversion is envisioned in spacetime regions where the hydrodynamic and particle descriptions are to good approximation equivalent, so we only switch 'language' but the state of the system is unchanged[11]. The particles are usually modeled as a gas, in which case one has to invert[39]

$$T^{\mu\nu}(x) \equiv \sum_i \int \frac{d^3p}{E} p^\mu p^\nu f_i(x,\mathbf{p}) \tag{2}$$

and

$$N_c^\mu(x) \equiv \sum_i q_{c,i} \int \frac{d^3p}{E} p^\mu f_i(x,\mathbf{p}) \ , \tag{3}$$

where $q_{c,i}$ is the charge of type c carried by a particle of species i.

For *non*dissipative fluids, which by definition are in local equilibrium everywhere in space at all times, the conversion is straightforward because in local thermal and chemical equilibrium particle distributions are[40]

$$f_i(x,\mathbf{p}) \equiv f_i^{\rm eq}(x,\mathbf{p}) = \frac{g_i}{(2\pi)^3} \exp\left[\frac{\mu_i(x) - p_\alpha u^\alpha(x)}{T(x)}\right] \quad , \qquad \mu_i \equiv \sum_c q_{c,i}\mu_c(x) \ , \tag{4}$$

where g_i is the number of internal degrees of freedom for species i. The combination $p_\alpha u^\alpha$ is the energy of the particle in the local rest (LR) frame of the fluid ($u^\mu_{LR} = (1,\mathbf{0})$). The local temperature T, chemical potentials $\{\mu_c\}$, and four-velocity u^μ of fluid flow are uniquely determined through the ideal hydrodynamic relations

$$T^{\mu\nu}_{\rm id}(x) = [e(x) + p(x)]u^\mu(x)u^\nu(x) - p(x)g^{\mu\nu} \quad , \qquad N^\mu_{c,{\rm id}}(x) = n_c(x)u^\mu(x) \ , \tag{5}$$

with $e(T,\{\mu_c\})$, $p(T,\{\mu_c\})$, and $n_c(T,\{\mu_c\})$ given by the equation of state (these can be inverted for T and $\{\mu_c\}$). For consistency, at the point of conversion the equation of state used in fluid dynamics must of course correspond to a gas of particles.

If the fluid is dissipative, then it is not strictly in local thermal and chemical equilibrium, and phase space densities therefore acquire dissipative corrections

$$f_i(x,\mathbf{p}) = f_i^{\rm eq}(x,\mathbf{p}) + \delta f_i(x,\mathbf{p}) \equiv f_i^{\rm eq}(x,\mathbf{p})[1+\phi_i(x,\mathbf{p})] \ . \tag{6}$$

The ideal hydrodynamic forms (5) no longer hold because the energy-momentum tensor and charge currents acquire nonideal corrections

$$T^{\mu\nu} = T^{\mu\nu}_{id} + \delta T^{\mu\nu} \quad , \qquad N^\mu_c = N^\mu_{c,{\rm id}} + \delta N^\mu_c \qquad\qquad (u_\mu \delta T^{\mu\nu} u_\nu = 0,\ u_\mu \delta N^\mu_c = 0) \ , \tag{7}$$

where $\delta T^{\mu\nu}$ is customarily decomposed further into a shear stress tensor $\pi^{\mu\nu}$ and bulk pressure Π:

$$\delta T^{\mu\nu} = \pi^{\mu\nu} + \Pi(u^\mu u^\nu - g^{\mu\nu}) \quad , \qquad \pi^\mu_\mu \equiv 0 \ , \tag{8}$$

if one uses Landau convention for fluid flow definition (so $u_\mu \delta T^{\mu\nu} \equiv 0$). On the other hand, (2) and (3) remain valid and can be recast as

$$\delta T^{\mu\nu}(x) = \sum_i \int \frac{d^3p}{E} p^\mu p^\nu \delta f_i(x,\mathbf{p}) \quad , \qquad \delta N^\mu_c(x) = \sum_i q_{c,i} \int \frac{d^3p}{E} p^\mu \delta f_i(x,\mathbf{p}) \ . \tag{9}$$

Without additional information about the functional form of the δf_i, this finite set of conditions can be satisfied with infinitely many different δf_i (or equivalently, ϕ_i), even if there is only a single particle species.

Often the only dissipative correction considered is shear stress. A common prescription that satisfies the constraint (9) from shear is the "democratic Grad" ansatz[5], which assumes phase space corrections with quadratic momentum dependence

$$\phi_i^{\rm dem}(x,\mathbf{p}) = \frac{\pi^{\mu\nu}(x)p_\mu p_\nu}{2[e(x)+p(x)]T^2(x)} \ . \tag{10}$$

Note, the coefficient in this quadratic form is the same for all particle species. The reason this ansatz works is that for each species it gives a partial shear stress that is proportional to the partial enthalpy:

$$\pi_i^{\mu\nu} \equiv \int \frac{d^3p}{E} p^\mu p^\nu \delta f_i^{\rm dem} = \frac{e_i+p_i}{e+p}\pi^{\mu\nu} \qquad \Rightarrow \qquad \sum_i \pi_i^{\mu\nu} = \pi^{\mu\nu} \ . \tag{11}$$

However, this simple choice ignores the very microscopic dynamics that keeps the gas near local equilibrium. In particular, one expects species that interact more frequently to be better equilibrated than those that scatter less often.

B. Covariant transport theory

In contrast, a self-consistent set of dissipative corrections can be obtained from linearized covariant transport theory. Consider on-shell covariant transport theory for a multicomponent system with $2 \to 2$ interactions. For each species i the evolution of the phase space density is given by the nonlinear Boltzmann transport equation

$$p^\mu \partial_\mu f_i(x,\mathbf{p}) = S_i(x,\mathbf{p}) + \sum_{jk\ell} C^{ij\to k\ell}[f_i,f_j,f_k,f_\ell](x,\mathbf{p}) \ , \tag{12}$$

where the source term S_i encodes the initial conditions, and the collision terms are[41]

$$C^{ij\to k\ell}[f_i,f_j,f_k,f_\ell](x,\mathbf{p}_1) \equiv \iiint\limits_{2\,3\,4} \left(\frac{g_i g_j}{g_k g_\ell} f_{3k} f_{4\ell} - f_{1i} f_{2j}\right) \bar{W}^{ij\to k\ell}_{12\to 34}\, \delta^4(12-34) \tag{13}$$

with shorthands $\int\limits_a \equiv \int d^3p_a/(2E_a)$, $f_{ai} \equiv f_i(x,\mathbf{p}_a)$, and $\delta^4(ab-cd) \equiv \delta^4(p_a+p_b-p_c-p_d)$. The transition probability $\bar{W}^{ij\to k\ell}_{12\to 34}$ for the process $i+j \to k+\ell$ with momenta $p_1+p_2 \to p_3+p_4$ is invariant under interchange of incoming or outgoing particles,

$$\bar{W}^{ij\to k\ell}_{12\to 34} \equiv \bar{W}^{ji\to k\ell}_{21\to 34} \equiv \bar{W}^{ij\to \ell k}_{12\to 43} \equiv \bar{W}^{ji\to \ell k}_{21\to 43} \ , \tag{14}$$

satisfies detailed balance

$$\bar{W}^{k\ell\to ij}_{34\to 12} \equiv \frac{g_i g_j}{g_k g_\ell} \bar{W}^{ij\to k\ell}_{12\to 34} \ , \tag{15}$$

and is given by the corresponding unpolarized scattering matrix element or differential cross section as

$$\bar{W}^{ij\to k\ell}_{12\to 34} = \frac{1}{16\pi^2} \overline{|\mathcal{M}^{ij\to k\ell}_{12\to 34}|^2} \equiv \frac{4}{\pi} s p_{cm}^2 \frac{d\sigma^{ij\to k\ell}_{12\to 34}}{dt} \equiv 4s \frac{p_{cm}}{p'_{cm}} \frac{d\sigma^{ij\to k\ell}_{12\to 34}}{d\Omega_{cm}} \ . \tag{16}$$

Here $s \equiv (p_1+p_2)^2$ and $t \equiv (p_1-p_3)^2$ are standard Mandelstam variables, while

$$p_{cm} \equiv \frac{\sqrt{(p_1p_2)^2 - m_i^2 m_j^2}}{\sqrt{s}} \qquad , \qquad p'_{cm} \equiv \frac{\sqrt{(p_3p_4)^2 - m_k^2 m_\ell^2}}{\sqrt{s}} \tag{17}$$

are the magnitudes of incoming and outgoing particle momenta in the center of mass frame of the microscopic two-body collision. The degeneracy factors g of the species appear explicitly in (15) because unpolarized matrix elements are summed over internal degrees of freedom (spin, polarization, color) of outgoing particles, whereas *averaged* over those of incoming particles. These factors also appear in (13) because distribution functions here are assumed to depend only on momentum and position but not on internal degrees of freedom, and thus the distribution of each species is summed over internal degrees of freedom (cf. the local equilibrium form (4)).

C. Self-consistent viscous corrections from linearized covariant transport

For small departures from local equilibrium one can split each phase space density into a local equilibrium part and a dissipative correction as in (6), and linearize (12) in δf:

$$p^\mu \partial_\mu f_i^{\rm eq} + p^\mu \partial_\mu \delta f_i = \sum_{jk\ell} \left\{ C^{ij\to k\ell}[\delta f_i, f_j^{\rm eq}, \delta f_k, f_\ell^{\rm eq}] + C^{ij\to k\ell}[f_i^{\rm eq}, \delta f_j, f_k^{\rm eq}, \delta f_\ell] \right\} \tag{18}$$

(with the source term dropped and spacetime and momentum arguments suppressed). The solutions to this coupled set of equations, of course, depend on both the matrix elements and initial conditions. However, typical systems quickly relax on microscopic scattering timescales to a solution dictated by gradients of the equilibrium distribution on the left hand side of (18). The asymptotic solution, for given gradients, is then uniquely determined by the interactions in the system (to see this relaxation worked out explicitly, check Ref. [12]). In this so-called Navier-Stokes regime, one can neglect the time derivative of δf_i, and if gradients of $f_i^{\rm eq}$ are small, one can also ignore[42] the spatial derivatives of δf_i. At each spacetime point x one then has a linear integral equation to solve. This is also the starting point of the standard calculation of transport coefficients in kinetic theory[13]. For example, the shear viscosity η_s and bulk viscosity ζ are defined in the Navier-Stokes limit through

$$\delta T^{\mu\nu}_{NS} \equiv \eta_s \sigma^{\mu\nu} + \zeta \Delta^{\mu\nu}(\partial u) \quad , \qquad \sigma^{\mu\nu} \equiv \nabla^\mu u^\nu + \nabla^\nu u^\mu - \frac{2}{3}\Delta^{\mu\nu}(\partial u) \ , \tag{19}$$

where $\Delta^{\mu\nu} \equiv g^{\mu\nu} - u^\mu u^\nu$ is a convenient projector to isolate spatial derivatives $\nabla^\mu = \Delta^{\mu\nu}\partial_\nu$ in the local rest (LR) frame.

The derivative on the LHS of (18) can be written as

$$\begin{aligned}(p\partial) f_i^{\rm eq} = \ f_i^{\rm eq} \ \Bigg\{ & p_\alpha \left[\nabla^\alpha \frac{\mu_i}{T} - (pu)\nabla^\alpha \frac{1}{T} \right] + (pu)(u\partial)\frac{\mu_i}{T} - (pu)^2 (u\partial)\frac{1}{T} \\ & - \frac{p_\alpha p_\beta}{2T} \left[\left(\nabla^\alpha u^\beta + \nabla^\beta u^\alpha - \frac{2}{3}\Delta^{\alpha\beta}(\partial u) \right) + \frac{2}{3}\Delta^{\alpha\beta}(\partial u) \right] - \frac{(pu)}{T} p_\alpha (u\partial) u^\alpha \Bigg\} \ . \end{aligned} \tag{20}$$

To isolate the response to shear, take uniform temperature and chemical potentials $T = const$, $\mu_c = const$, with $\sigma^{\mu\nu} \neq 0$ but $(\partial u) = 0$. Only terms on the second line remain; the ones in the square bracket contribute to $\delta T^{\mu\nu}$, whereas the last term with temporal derivative $(u\partial)$ can be dropped as long as gradients are weak[43]. With symmetric, traceless, purely spatial (in LR), and dimensionless tensors

$$P^{\mu\nu} \equiv \frac{1}{T^2}\left[\Delta^\mu_\alpha \Delta^\nu_\beta p^\alpha p^\beta - \frac{1}{3}\Delta^{\mu\nu}(\Delta_{\alpha\beta} p^\alpha p^\beta) \right] \ , \quad X^{\mu\nu} \equiv \frac{\sigma^{\mu\nu}}{T} = \frac{\pi^{\mu\nu}_{NS}}{\eta_s T} \ , \tag{21}$$

we then have

$$(p\partial) f_i^{\rm eq} = -\frac{T^2}{2} f_i^{\rm eq} P^{\mu\nu}(p) X_{\mu\nu}(x) \ . \tag{22}$$

The RHS of (18) simplifies upon the realization (see Appendix A and Refs. [14, 15]) that

$$\phi_i(x,\mathbf{p}) = \chi_i(|\tilde{\mathbf{p}}|) P^{\mu\nu} X_{\mu\nu} \qquad \text{with} \quad \frac{1}{T}\Delta^{\mu\nu} p_\nu \Big|_{LR} \equiv (0, \tilde{\mathbf{p}}) \ , \tag{23}$$

where $\tilde{\mathbf{p}}$ is the LR frame three-momentum normalized by temperature. This means that δf_i are solely determined by real, dimensionless scalar functions χ_i of the rescaled momentum. Substituting (23) and (22) into (18) yields, with the help of

$$\frac{g_i g_j}{g_k g_\ell} f_{3k}^{\rm eq} f_{4\ell}^{\rm eq} \delta^4(12-34) \equiv f_{1i}^{\rm eq} f_{2j}^{\rm eq} \delta^4(12-34) \ , \tag{24}$$

the integral equation

$$-\frac{1}{2} P_1^{\mu\nu} f_{1i}^{\rm eq} = \frac{1}{T^2} \sum_{jk\ell} \iiint_{2\,3\,4} f_{1i}^{\rm eq} f_{2j}^{\rm eq} \, \bar{W}^{ij\to k\ell}_{12\to 34} \, \delta^4(12-34) \left(\chi_{3k} P_3^{\mu\nu} + \chi_{4\ell} P_4^{\mu\nu} - \chi_{1i} P_1^{\mu\nu} - \chi_{2j} P_2^{\mu\nu} \right) \ , \tag{25}$$

which after contraction with $P_{1,\mu\nu}$ reads

$$-\frac{1}{2}P_1\cdot P_1 f_{1i}^{\rm eq} = \frac{1}{T^2}\sum_{jk\ell}\iiint_{2\,3\,4} f_{1i}^{\rm eq} f_{2j}^{\rm eq}\,\bar{W}_{12\to 34}^{ij\to k\ell}\,\delta^4(12-34)\,(\chi_{3k}P_3\cdot P_1+\chi_{4\ell}P_4\cdot P_1-\chi_{1i}P_1\cdot P_1-\chi_{2j}P_2\cdot P_1) \tag{26}$$

if one introduces the notation

$$\chi_{ai}\equiv\chi_i(|\tilde{\mathbf{p}}_a|)\quad,\qquad P_a\cdot P_b\equiv P_a^{\mu\nu}P_{b,\mu\nu}=(\tilde{\mathbf{p}}_a\tilde{\mathbf{p}}_b)^2-\frac{1}{3}|\tilde{\mathbf{p}}_a|^2|\tilde{\mathbf{p}}_b|^2\ . \tag{27}$$

It is straightforward to show with the help of (14), (15) and (24) that (26) is equivalent to the extremization of the functional

$$\begin{aligned} Q[\chi] \;&=\; \frac{1}{2T^2}\sum_i\int_1 P_1\cdot P_1 f_{1i}^{\rm eq}\chi_{1i} \\ &\quad+\frac{1}{2T^4}\sum_{ijk\ell}\iiiint_{1\,2\,3\,4} f_{1i}^{\rm eq} f_{2j}^{\rm eq}\,\bar{W}_{12\to 34}^{ij\to k\ell}\,\delta^4(12-34)\,(\chi_{3k}P_3\cdot P_1+\chi_{4\ell}P_4\cdot P_1-\chi_{1i}P_1\cdot P_1-\chi_{2j}P_2\cdot P_1)\chi_{1i} \\ &\equiv\; \sum_i B_i+\sum_{ijk\ell}(Q_{31}^{ij\to k\ell}+Q_{41}^{ij\to k\ell}-Q_{11}^{ij\to k\ell}-Q_{21}^{ij\to k\ell})\ , \end{aligned} \tag{28}$$

i.e., (26) is reproduced by the usual variational procedure imposing $\delta Q[\chi]=0+\mathcal{O}(\delta\chi^2)$. This allows one to estimate χ_i variationally using a finite basis $\{\Psi_{i,n}\}$ as

$$\chi_i(|\tilde{\mathbf{p}}|)=\sum_n c_{i,n}\Psi_{i,n}(|\tilde{\mathbf{p}}|) \tag{29}$$

and finding optimal coefficients $\{c_{i,n}\}$ that maximize Q (one can in principle use different Ψ_n for different species). If the basis is complete, the limit $n\to\infty$ reproduces the exact solution. Numerical evaluation of Q is discussed in Appendix B.

The extremal value of Q is directly related to the shear viscosity. Comparison of (19) to (9) with (23) gives

$$\eta_s=\frac{T_{LR}^{xz}}{\sigma_{LR}^{xz}}=\frac{2}{15T^3}\sum_i\int\frac{d^3p}{E}p^4 f_i^{\rm eq}\chi_i=\frac{4T^3}{5}\sum_i B_i \tag{30}$$

with B_i from (28). On the other hand, from (26) it follows that for the exact solution

$$-\sum_i B_i=2\sum_{ijk\ell}(Q_{31}^{ij\to k\ell}+Q_{41}^{ij\to k\ell}-Q_{11}^{ij\to k\ell}-Q_{21}^{ij\to k\ell})\ , \tag{31}$$

i.e., the maximum of Q is $Q_{max}=\sum_i B_i/2$. Thus, the shear viscosity is

$$\eta_s=\frac{8}{5}Q_{max}T^3\ . \tag{32}$$

From (23), (29) and (21) one concludes that the democratic Grad ansatz (10) corresponds to a single momentum independent (constant) basis function with coefficient $c_i=1$, i.e.,

$$\chi_i^{\rm dem}=c_i\frac{\eta_s T}{2(e+p)}=\frac{\eta_s}{2s} \tag{33}$$

for all species, where in the last step the thermodynamic identity $Ts=e+p-\sum_c\mu_c n_c$ was employed with vanishing chemical potentials appropriate for the midrapidity region in heavy-ion collisions at RHIC and LHC energies. Except for the factor of 1/2, the common $\chi_i^{\rm dem}$ value is then just the shear viscosity to entropy ratio. In the following we study the species dependence of χ_i from microscopic dynamics.

III. MASSLESS TWO-COMPONENT SYSTEM

Consider the so-called Grad approximation, in which

$$\chi_i(|\tilde{\mathbf{p}}|) = \chi_i^{Grad} = const \ , \tag{34}$$

i.e., phase space corrections ϕ_i are quadratic in momentum. For massless particles with energy-independent, isotropic cross sections, the terms in $Q[\chi]$ readily evaluate to (see Appendix B)

$$\begin{aligned} B_i &= 10\frac{n_i}{T^3}\chi_i \ , \qquad Q_{11}^{ij\to k\ell} = 30(1+\delta_{k\ell})\frac{\sigma_{TOT}^{ij\to k\ell} n_i n_j}{T^4}\chi_i^2 \ , \qquad Q_{21}^{ij\to k\ell} = 0 \\ Q_{31}^{ij\to k\ell} &= \frac{20}{3}(1+\delta_{k\ell})\frac{\sigma_{TOT}^{ij\to k\ell} n_i n_j}{T^4}\chi_i\chi_k \ , \qquad Q_{41}^{ij\to k\ell} = \frac{20}{3}(1+\delta_{k\ell})\frac{\sigma_{TOT}^{ij\to k\ell} n_i n_j}{T^4}\chi_i\chi_\ell \ , \end{aligned} \tag{35}$$

where we used (B4), (B5), and (B11) with $E_a = p_a$, $\gamma_3 = \beta_3 = 1/2$, and substituted equilibrium densities

$$n_i = \frac{g_i}{\pi^2}T^3 e^{\mu_i/T} \ . \tag{36}$$

For a one-component massless system,

$$Q[\chi] = \frac{10n}{T^3}\chi\left(1 - \frac{10n\sigma_{TOT}}{3T}\chi\right) \ , \tag{37}$$

which is maximal at $\chi^{Grad} = 3T\lambda_{MFP}/20$, where $\lambda_{MFP} = 1/n\sigma_{TOT}$ is the mean free path. So the viscous correction is a dimensionless measure of the mean free path in this case. The corresponding shear viscosity from (32) is the well-known Grad result $\eta_s = 6T/5\sigma_{TOT}$.

A. Two-component system in Grad approximation

Extension to a minimalist multicomponent system with two massless species and elastic two-body interactions involves three interaction channels $A+A \to A+A$, $B+B \to B+B$, and $A+B \to A+B$. Crossing symmetry would also imply inelastic $A+A \to B+B$ and $B+B \to A+A$ but these are ignored here in order to isolate shear only (if particle densities are allowed to change, there will also be dissipative effects due to particle diffusion). With isotropic, energy-independent cross sections σ_{AA}, σ_{BB}, and σ_{AB}, for this system in Grad approximation,

$$Q = \frac{10}{T}(n_A\chi_A + n_B\chi_B) - \frac{100}{3T^4}(\sigma_{AA}n_A^2\chi_A^2 + \sigma_{BB}n_B^2\chi_B^2) + \frac{20\sigma_{AB}n_A n_B}{3T^4}(4\chi_A\chi_B - 7\chi_A^2 - 7\chi_B^2) \ , \tag{38}$$

which is maximized when

$$\begin{aligned} \chi_A^{Grad} &= \frac{3LT}{20}\frac{5K_{B(B)} + 7K_{B(A)} + 2K_{A(B)}}{K_{A(A)}[5K_{B(B)} + 7K_{B(A)}] + K_{A(B)}[9K_{B(A)} + 7K_{B(B)}]} \\ \chi_B^{Grad} &= \frac{3LT}{20}\frac{5K_{A(A)} + 7K_{A(B)} + 2K_{B(A)}}{K_{B(B)}[5K_{A(A)} + 7K_{A(B)}] + K_{B(A)}[9K_{A(B)} + 7K_{A(A)}]} \ . \end{aligned} \tag{39}$$

Here $K_{i(j)} \equiv L/\lambda_{i(j)} = Ln_j\sigma_{ij}$ denote partial inverse Knudsen numbers characterizing scattering of species i off species j and L is the characteristic length scale for gradients in the system. All four $K_{i(j)}$ play a role because the solution to (26) is influenced by any particle in the microscopic scattering process that is out of equilibrium (whether incoming, or outgoing). The partial inverse Knudsen numbers also come with different weights, therefore, unlike for a single-component system, the result cannot in general be reproduced with just the mean free path as $\chi_i \sim T\lambda_i \equiv LT/K_i = LT/\sum_j K_{i(j)}$. The Grad estimate of the shear viscosity

$$\eta_s^{Grad} = \frac{6T}{5}\frac{\sigma_{AB}(7r + 7r^{-1} + 4) + 5(\sigma_{AA} + \sigma_{BB})}{7\sigma_{AB}(\sigma_{AA}r + \sigma_{BB}r^{-1}) + 9\sigma_{AB}^2 + 5\sigma_{AA}\sigma_{BB}} \quad , \qquad r \equiv \frac{n_A}{n_B} \tag{40}$$

from (32) is strictly speaking a variational lower bound on the exact η_s value but usually reasonably accurate in practice (for the isotropic cross sections used here).

B. Comparison to nonlinear transport with 0+1D Bjorken expansion

Linearized transport results correspond to the Navier-Stokes limit where the system relaxed to a solution dictated by gradients of hydrodynamic variables. For expanding systems, such as those in heavy-ion collisions, relaxation to local equilibrium has to compete with dilution and cooling, therefore it is important to check how well the limit applies when local equilibrium is no longer a static fixed point in time.

A convenient test scenario is a massless system undergoing boost-invariant 0+1D Bjorken expansion[44] with homogeneous and isotropic transverse directions (x, y), just like in Ref. [16] but with a two-component $A+B$ mixture. The system starts out at longitudinal proper time $\tau \equiv \sqrt{t^2 - z^2} = \tau_0$ in local thermal equilibrium but due to expansion dissipative corrections quickly develop and can be easily quantified using the partial shear stresses of the two species. Due to scaling of the transport solutions[17] the evolution only depends on the dimensionless ratio $\tilde{\tau} \equiv \tau/\tau_0$ and partial inverse Knudsen numbers $K_{i(j)} \equiv \tau/\lambda_{i(j)} = \tau n_j \sigma_{ij}$, where the characteristic scale for gradients is the proper time τ. The initial temperature T_0 does not play any role beyond setting the momentum scale (all momenta are proportional to T_0). As in Section III A, we only include elastic two-body interactions $A+A \to A+A$, $B+B \to B+B$, and $A+B \to A+B$. All three cross sections are set to grow with time as $\sigma_{ij} \propto \tau^{2/3}$, which ensures[45] approximately scale invariant dynamics with $\eta_s/s \approx const$. In such a scenario, longitudinal expansion first drives the system out of local equilibrium but at late times the system returns, asymptotically, to local equilibrium.

By symmetry, the phase space densities $f_i(\tau, p_T, \xi)$ only depend on proper time τ, transverse momentum magnitude p_T, and the difference $\xi \equiv \eta - y$ between coordinate rapidity η and momentum rapidity y (see Appendix E for definitions). The flow velocity is constrained to $u^\mu = (\mathrm{ch}\,\eta, 0, 0, \mathrm{sh}\,\eta)$, and for both species shear stress is diagonal in the LR ($\eta = 0$) frame, i.e.,

$$\pi^{\mu\nu}_{i,LR} = diag(0, -\pi_{L,i}/2, -\pi_{L,i}/2, \pi_{L,i}) \ , \tag{41}$$

where $\pi_{L,i}$ is the longitudinal shear stress for species i. Assuming dissipative corrections are quadratic in momentum, we have

$$\phi_i = c_i \frac{\pi^{\mu\nu} p_\mu p_\nu}{2(e+p)T^2} = c_i(\tilde{\tau}) \frac{\pi_L(\tilde{\tau})}{8p(\tilde{\tau})} \frac{p_T^2}{T^2(\tilde{\tau})} \left(\mathrm{sh}^2\xi - \frac{1}{2} \right) \quad \Rightarrow \quad c_i(\tilde{\tau}) = \frac{\pi_{L,i}(\tilde{\tau})}{p_i(\tilde{\tau})} \frac{p(\tilde{\tau})}{\pi_L(\tilde{\tau})} \ , \tag{42}$$

where $e_i = 3p_i$ was substituted for massless particles. Up to the factor p/π_L that is common to all species, c_i describes how far species i is from local equilibrium. In the late-time Navier-Stokes regime, linearized kinetic theory predicts

$$\frac{c_B}{c_A} = \frac{5K_A + 2(K_{A(B)} + K_{B(A)})}{5K_B + 2(K_{A(B)} + K_{B(A)})} \qquad (K_i \equiv \sum_j K_{i(j)}) \tag{43}$$

(cf. (33) and (39), and note that the denominators in (39) cancel in the ratio). The "democratic Grad" approach on the other hand postulates $c_i = 1$ for all species, so $c_B/c_A = 1$.

Figure 1 compares these two extremes to fully nonlinear transport solutions obtained using Molnar's Parton Cascade (MPC) [18]. The simulations are initialized with uniform coordinate rapidity distributions $dN/d\eta$ in a wide window $|\eta| < 5$. To avoid the $|\eta| \gtrsim 4$ edges of the system where boost invariance is strongly violated, shear stress evolution is extracted only using particles with $|\eta| < 2$ (all boosted to the $\eta = 0$ frame). A variety of relative cross sections and densities between the two species are explored in five different scenarios shown in Table I, which all keep species A closer to equilibrium than B. In all five cases, the ratio of viscous corrections c_B/c_A starts from unity but then relaxes to a constant value at late times that depends on the partial inverse Knudsen numbers in the system. While the commonly used "democratic Grad" ansatz fails to account for the species dependence of viscous corrections, linearized transport (Eq. (43)) captures the corrections with better than 10% accuracy in all five scenarios despite rapid longitudinal expansion.

Shear stress evolution in a particle mixture has also been studied in [19], albeit using a different approach based on imposing the second law of thermodynamics (entropy production). In that work, an approximate relation for partial shear stress ratios has also been obtained (cf. (12) therein). While that result qualitatively captures both the rise and saturation of the curves in Fig. 1, quantitatively, the predicted asymptotic values are not identical to (43) here. However, those results are for an assumed uniform flow velocity across the entire system, which is inconsistent with $\pi^{\mu\nu} \sim \nabla^\mu u^\nu$ in the Navier-Stokes regime considered here. It would be interesting to compare these two approaches in more detail in the future.

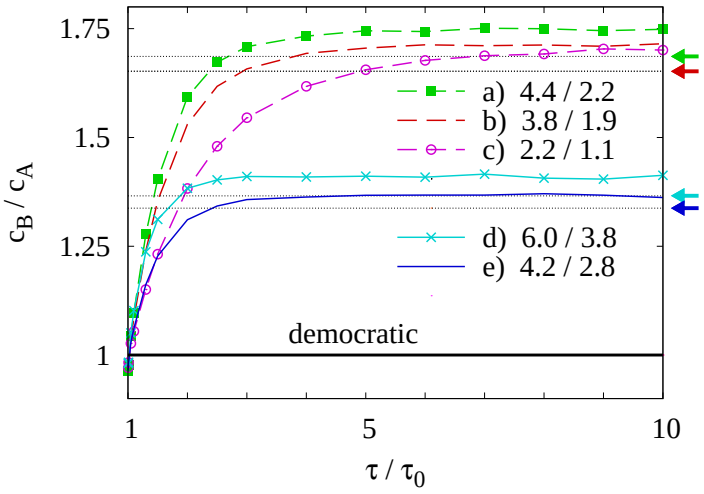

FIG. 1: Ratio of dissipative corrections as a function of normalized proper time for a massless two-component system in a 0+1D Bjorken scenario, calculated from nonlinear $2 \to 2$ covariant transport using MPC[18]. Five different scenarios a) - e) with various cross sections and densities are shown, labeled with the ratio of inverse Knudsen numbers K_A/K_B. See Table I for a detailed list of parameters. Thin, horizontal dotted lines and arrows on the right side of the plot correspond to the expectation from a self-consistent calculation based on linearized transport in the quadratic Grad approximation ("dynamical Grad" approach). Only four such lines and arrows are visible because scenarios b) and c) are identical except for the timescale of relaxation to Navier-Stokes regime; scenario b) relaxes 5/3 times quicker than c).

TABLE I: Inverse Knudsen numbers for the two species, and ratios of densities and cross sections, for the two-component massless covariant transport calculation in Fig. 1.

Scenario	K_A	K_B	$n_A : n_B$	$\sigma_{AA} : \sigma_{AB} : \sigma_{BB}$
a)	4.4	2.2	3 : 1	20 : 10 : 5
b)	3.8	1.9	2 : 2	20 : 10 : 5
c)	2.2	1.1	2 : 2	12 : 6 : 3
d)	6	3.8	1 : 3	24 : 24 : 12
e)	4.2	2.8	2 : 2	20 : 13.3 : 8.89

IV. MASSIVE TWO-COMPONENT SYSTEM

For nonrelativistic particles, in the Grad approximation (see Appendix D),

$$
\begin{aligned}
B_i &= \frac{5 z_i}{2} \frac{n_i}{T^3} \chi_i \\
Q_{11}^{ij\to k\ell} &= \frac{1}{3\sqrt{2\pi}} \frac{z_i^{3/2}}{z_j^{1/2}} \frac{15 z_i^2 + 40 z_i z_j + 24 z_j^2}{(z_i + z_j)^{3/2}} (1 + \delta_{k\ell}) \frac{\sigma_{TOT}^{ij\to k\ell} n_i n_j}{T^4} \chi_i^2 \\
Q_{21}^{ij\to k\ell} &= -\frac{1}{3\sqrt{2\pi}} \left(\frac{z_i z_j}{z_i + z_j} \right)^{3/2} (1 + \delta_{k\ell}) \frac{\sigma_{TOT}^{ij\to k\ell} n_i n_j}{T^4} \chi_i \chi_j \\
Q_{31}^{ij\to k\ell} &= \frac{5}{\sqrt{2\pi}} \frac{z_i^{3/2} z_k^2}{z_j^{1/2} (z_i + z_j)^{3/2}} (1 + \delta_{k\ell}) \frac{\sigma_{TOT}^{ij\to k\ell} n_i n_j}{T^4} \chi_i \chi_k \\
Q_{41}^{ij\to k\ell} &= \frac{5}{\sqrt{2\pi}} \frac{z_i^{3/2} z_\ell^2}{z_j^{1/2} (z_i + z_j)^{3/2}} (1 + \delta_{k\ell}) \frac{\sigma_{TOT}^{ij\to k\ell} n_i n_j}{T^4} \chi_i \chi_\ell
\end{aligned}
\tag{44}
$$

where $z \equiv m/T$ and equilibrium densities

$$n_i^{NR} = \frac{g_i}{(2\pi)^{3/2}}(m_i T)^{3/2} e^{(\mu_i - m_i)/T} \tag{45}$$

were substituted. For a one-component nonrelativistic system, the above imply

$$\chi^{Grad} = \frac{5\sqrt{\pi}}{32}\sqrt{\frac{T}{m}}\frac{T}{n\sigma_{TOT}} \quad \Rightarrow \quad \eta_s^{Grad} = \frac{5\sqrt{\pi}}{16}\frac{\sqrt{mT}}{\sigma_{TOT}} \, , \tag{46}$$

reproducing the familiar nonrelativistic viscosity expression. Notice that for fixed density and cross section the relative viscous correction $\delta f/f^{\rm eq}$ *decreases* when mass increases, even though shear viscosity increases with mass.

For a one-component system the shear viscosity is known analytically, in Grad approximation, for arbitrary m/T with fully relativistic kinematics (see Chapter XI of Ref. [14]):

$$\eta_s^{Grad} = \frac{15 z^2 K_2^2(z) h^2(z)}{16[(15z^2+2)K_2(2z) + (3z^3+49z)K_3(2z)]}\frac{T}{\sigma_{TOT}} \qquad , \qquad h(z) \equiv z K_3(z)/K_2(z) \, , \tag{47}$$

where K_n is a modified Bessel function of the second kind. The numerical integration method in Appendix B reproduces this result, and we also rechecked the complete derivation of the formula in Ref. [14] (note the typographic error in the book; the correct coefficient in the denominator is 15, not 5).

A. Two-component nonrelativistic system in Grad approximation

For a two-component nonrelativistic $A+B$ system with isotropic, energy-independent, elastic scattering, in Grad approximation

$$Q[\chi_A, \chi_B] = \left[\frac{5 z_A n_A \chi_A}{2T^3} - \frac{8\sigma_{AA} n_A^2 z_A^{3/2} \chi_A^2}{\sqrt{\pi} T^4} + \frac{8\sqrt{2}\,\sigma_{AB} n_A n_B z_A^{3/2} z_B^{1/2}[(5z_A+3z_B)\chi_A - 2z_B\chi_B]\chi_A}{3\sqrt{\pi}T^4(z_A+z_B)^{3/2}} \right] + A \leftrightarrow B \, . \tag{48}$$

The general structure of the solution is very similar to the massless case, namely, all partial inverse Knudsen numbers contribute with different weights that now also depend on the masses. In the limit when species B is much more dilute than species A (for example, because it is very heavy), we can approximate $n_B \to 0$ to obtain

$$\begin{aligned} \chi_A^{Grad}\big|_{n_B\to 0} &= \frac{5\sqrt{\pi}}{32}\sqrt{\frac{T}{m_A}}\frac{T}{\sigma_{AA} n_A} \quad , \\ \chi_B^{Grad}\big|_{n_B\to 0} &= \chi_A^{Grad}\frac{3(\mu+1)^2\sigma_{AA} + 2\sqrt{2\mu(1+\mu)}\sigma_{AB}}{\sqrt{2\mu(1+\mu)}(3+5\mu)\sigma_{AB}} \qquad (\mu = \frac{m_B}{m_A}) \, . \end{aligned} \tag{49}$$

In this special case species A is unaffected by species B, and also σ_{BB} is irrelevant. On the other hand, for species B we have

$$\begin{aligned} \frac{\chi_B}{\chi_A} &= \frac{3\sigma_{AA}}{4\sigma_{AB}} + \frac{1}{4} \qquad \text{if} \quad m_A = m_B, \\ \frac{\chi_B}{\chi_A} &\approx \frac{3\sigma_{AA}}{5\sqrt{2}\,\sigma_{AB}} \qquad \text{if} \quad m_B \gg m_A \, , \end{aligned} \tag{50}$$

which tells that the heavier species tends to have *smaller* viscous correction even when its interaction cross section is the same as that of the light species.

B. Pion-nucleon gas and elliptic flow

Next consider a more realistic pion-nucleon system, with relativistic kinematics. Lumping isospin states and antiparticles into a single species, this is a two-component system with $m_\pi = 0.14$ GeV, $g_\pi = 3$, $m_N = 0.94$ GeV, $g_N = 4$. For temperatures 120 MeV $\lesssim T \lesssim$ 165 MeV of interest we approximate the two-body cross sections with constant, energy-independent, effective values $\sigma_{\pi\pi}^{eff} = 30$ mb, $\sigma_{\pi N}^{eff} = 50$ mb, and $\sigma_{NN}^{eff} = 20$ mb. These values are set

TABLE II: Mean scattering times in a pion-nucleon gas with effective cross sections $\sigma_{\pi\pi}^{eff} = 30$ mb, $\sigma_{\pi N}^{eff} = 50$ mb, and $\sigma_{NN}^{eff} = 20$ mb. Values are rounded to the two most significant digits.

T [MeV]	$\bar{\tau}_{\pi\pi}$ [fm]	$\bar{\tau}_{N(\pi)}$ [fm]	$\bar{\tau}_{NN}$ [fm]
100	12.7	8.2	8300
120	6.6	4.2	1200
140	3.9	2.4	280
165	2.2	1.4	73
200	1.2	0.73	18

so that for a static system ($u^\mu = (1, \mathbf{0})$) in thermal and chemical equilibrium the mean times $\bar{\tau}_{i(j)}$ between scatterings for particles of species i with particles of species j, defined through

$$\frac{1}{\bar{\tau}_{i(j)}} = \langle n_j \sigma_{ij} v_{rel} \rangle = \frac{1}{n_i} \int \frac{d^3p_1}{E_1} \frac{d^3p_2}{E_2} f_i^{\rm eq}(\mathbf{p}_1) f_j^{\rm eq}(\mathbf{p}_2) \sigma_{ij} F(s) \ , \tag{51}$$

are comparable to the values shown in Figs. 2b and 5a of Ref. [20] (Table II lists the mean scattering times with these effective cross sections as a function of temperature, including $T = 100$ and 200 MeV outside the matching range). Here

$$F(s) \equiv p_{cm}\sqrt{s} \equiv E_1 E_2 v_{rel} = \frac{1}{2}\sqrt{(s - m_i^2 - m_j^2)^2 - 4m_i^2 m_j^2} \tag{52}$$

is the flux factor. Note that at these temperatures pions are much more abundant than nucleons, and therefore nucleon-nucleon scattering affects viscous corrections negligibly (one could put $\sigma_{NN} = 0$ to good approximation).

For the $\pi - N$ system, the ratio of viscous coefficients is $c_\pi/c_N \sim 2$ in the temperature window $100 < T < 200$ MeV, as shown in Figure 2. This means that nucleons are about twice as close as pions to equilibrium (at the same momentum), in qualitative agreement with the analytic results in Section IV. For example, the nonrelativistic formula (49) would predict $c_\pi/c_N \approx 2.9$, which is not bad considering that pions are relativistic at these temperatures. The primary origin of the pion-nucleon difference is the larger πN cross section – a nucleon scatters more frequently off pions than a pion scatters off another pion. But based on the earlier discussion one would expect $c_\pi > c_N$ even for $\sigma_{\pi\pi} = \sigma_{\pi N}$.

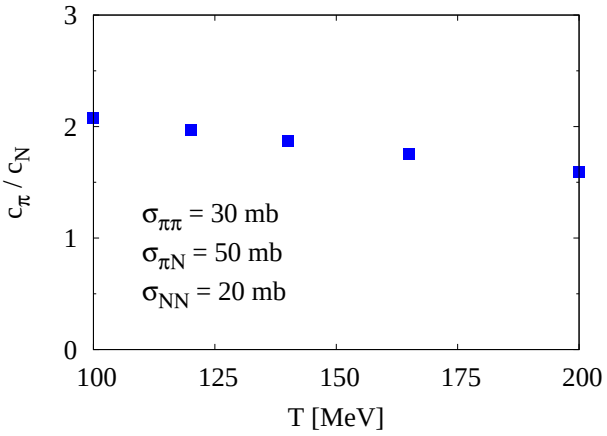

FIG. 2: Self-consistent dissipative corrections for shear stress as a function of temperature for a chemically equilibrated pion-nucleon gas, in the Grad approximation, with effective cross sections $\sigma_{\pi\pi}^{eff} = 30$ mb, $\sigma_{\pi N}^{eff} = 50$ mb, and $\sigma_{NN}^{eff} = 20$ mb. The ratio of coefficients c_π/c_N is shown, where c_i is the dissipative correction for species i *relative* to the commonly used "democratic" ansatz (see text).

The above pion-nucleon difference is reflected in pion vs proton observables if the self-consistent, species-dependent viscous corrections are included in Cooper-Frye freezeout. To estimate the effect, we perform a hydrodynamic simulation of $Au + Au$ at top RHIC energy $\sqrt{s_{NN}} = 200$ GeV with impact parameter $b = 7$ fm, and look at the

difference between pion and proton elliptic flow. The calculations are done with AZHYDRO [21, 22] version 0.2p2, which is a 2+1D code with longitudinal boost invariance. This version includes the fairly recent s95-p1 equation of state parameterization[23] by Huovinen and Petreczky that matches lattice QCD results to a hadron resonance gas. Because there is no dissipation in AZHYDRO, we estimate shear stress on the conversion hypersurface from gradients of the ideal flow fields using the Navier-Stokes formula (19), i.e., $\pi^{\mu\nu} = \eta_s \sigma^{\mu\nu}$. This is in the same spirit as an early exploration of shear stress corrections by Teaney [24], except we use real hydrodynamic solutions instead of a parameterization. We set $\eta_s/s = 0.1$, and determine the shear viscosity from the hydrodynamic solutions using

$$\eta_s = \frac{\eta_s}{s}\frac{e+p}{T} \qquad (\mu_B = 0)\ . \tag{53}$$

For initial conditions at Bjorken proper time $\tau_0 = 0.5$ fm we set the transverse entropy density distribution $ds/d^2x_T d\eta$ to a 25%+75% weighted sum of binary collision and wounded nucleon profiles ($\sigma_{NN}^{inel} = 40$ mb), with diffuse Woods-Saxon nuclear densities for gold nuclei (Woods-Saxon parameters $R = 6.37$ fm, $\delta = 0.54$ fm), a peak entropy density value $s_0 = \frac{1}{\tau_0}\frac{ds(\mathbf{x}_T=0)}{d^2x_T d\eta} = 110/\mathrm{fm}^3$, and vanishing baryon density $n_B = 0$ everywhere. With ordinary, ideal ($\delta f = 0$) Cooper-Frye freezeout at temperature $T_{conv} = 140$ MeV, this roughly reproduces the measured pion spectrum. In the following we keep the initial conditions fixed but vary T_{conv}, and study pion and proton elliptic flow from fluid-to-particle conversion with self-consistent viscous δf corrections. The viscous Cooper-Frye procedure is discussed in Appendix E (the AZHYDRO code only handles ideal freezeout, i.e., $\delta f = 0$).

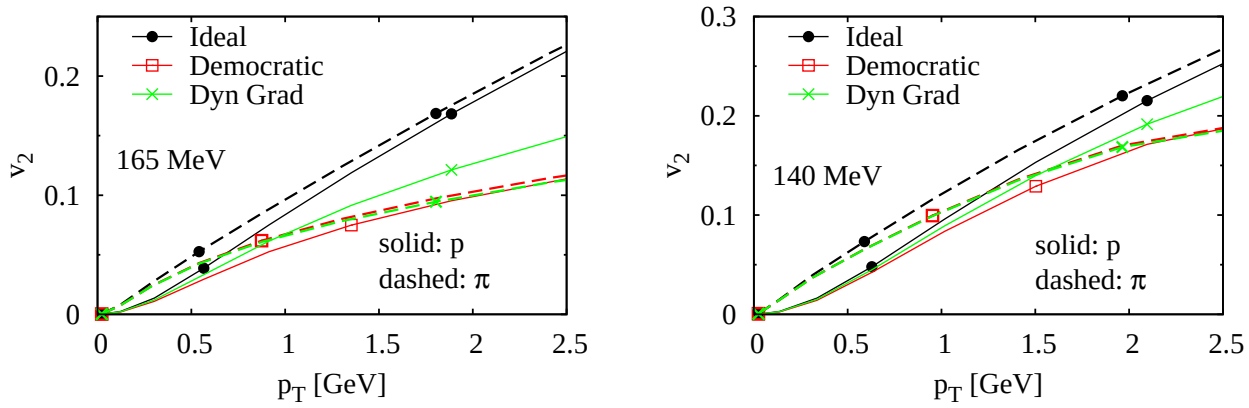

FIG. 3: Differential elliptic flow $v_2(p_T)$ of pions and protons in $Au+Au$ at $\sqrt{s_{NN}} = 200$ GeV at RHIC with impact parameter $b = 7$ fm, using 2+1D boost invariant hydrodynamic solutions from AZHYDRO[21, 22], and Cooper-Frye fluid-to-particle conversion at $T_{conv} = 165$ MeV (left plot) or 140 MeV (right plot). Dashed lines are for pions, while solid curves are for protons. The standard "democratic Grad" approach (open boxes) is compared to self-consistent shear corrections (crosses) computed for a pion-nucleon gas from linearized kinetic theory (see text). In both cases, $\eta_s/s = 0.1$ at conversion. Results with uncorrected, local equilibrium phase space distributions ($\delta f = 0$) are also shown (filled circles).

The left plot in Figure 3 shows differential elliptic flow results for pions and protons for freezeout at $T_{conv} = 165$ MeV. Pion and proton v_2 separate already in the ideal case (filled circles), following the characteristic mass ordering of v_2 in hydro. At high p_T this effect diminishes, however. Viscous freezeout with the commonly used democratic ansatz (open boxes) preserves the mass ordering but with v_2 strongly suppressed by dissipation, even for the modest $\eta_s/s = 0.1$ used here. In this calculation dissipative effects are only present in the viscous phase space corrections δf_i at fluid-to-particle conversion but viscous corrections to the evolution of hydrodynamic flow and temperature fields are known[7, 25, 26] to have smaller influence on v_2 then δf itself. In contrast, self-consistent species-dependent freezeout (crosses) leads to a clear pion-proton elliptic flow splitting at moderately high transverse momenta, with the proton v_2 exceeding the pion v_2 by 30%. Both species exhibit a strong viscous suppression in v_2. However, the suppression is smaller for protons because they are more equilibrated than pions. At low p_T the mass effect is still present, which means that the pion and proton elliptic flow curves necessarily cross each other (at around $p_T \sim 1$ GeV in this calculation). The reason why the pion results are almost identical to "democratic" freezeout is that at $T = 165$ MeV the pion density is much higher than the proton density, i.e., the dynamics of pions is largely unaffected by the protons, and both the shear viscosity and the entropy density are then dominated by pions. The temperature $T = 165$ MeV used here is the same as the typical switching temperature in hybrid hydro+transport models[4]. It would be very interesting to initialize the transport stage of hybrid calculations with self-consistent viscous distributions for each species, and check the effect on identified particle elliptic flow at the end of the hadron transport evolution.

The right plot of Fig. 3 shows the same $v_2(p_T)$ calculation but with a lower $T_{conv} = 140$ MeV. The qualitative picture is the same, but in this case the viscous suppression of v_2 is smaller in magnitude because, for the Navier-Stokes stresses (19) used here, flow gradients $\partial^\mu u^\nu \sim 1/\tau$ are smaller. The mass ordering is also stronger, which is expected because it is driven by m/T. At the same $p_T \sim 2-2.5$ GeV, the relative difference between proton v_2 curves from the "democratic" and the self-consistent approaches is smaller than for $T_{conv} = 165$ MeV. However, the relative *change* in viscous suppression of v_2 is actually larger; the difference for protons between ideal hydrodynamic flow and the viscous result shrinks by a factor of two at $T_{conv} = 140$ MeV when the fluid is converted to particles with the self-consistent (species-dependent) scheme.

At even lower temperature $T_{conv} = 120$ MeV, dissipative corrections for $\eta_s/s = 0.1$ are basically negligible for protons for $p_T < 2.5$ GeV, at least with the Navier-Stokes shear stress used here. For pions there is a less then 10% suppression in v_2 at high p_T.

C. Simple four-source model of viscous elliptic flow

The elliptic flow results presented in Sec. IV B come from numerical hydrodynamic solutions, where both inhomogeneities over the Cooper-Frye hypersurface and also the shape of the hypersurface matter. It is desirable to gain at least some qualitative analytic insight into how viscous corrections affect differential $v_2(p_T)$ for particles of different masses. To this end we generalize the simple model in [32] (cf. Fig. 6 therein), which considered four uniform, non-expanding fireballs boosted symmetrically in back-to-back pairs along the x and y directions in the transverse plane, respectively, with velocities $\pm v_x$ and $\pm v_y$ ($v_x > v_y \geq 0$). All four sources have the same temperature, chemical potential, and volume in the laboratory frame. Isochronous $t = const$ emission is considered at zero momentum rapidity, in which case flow coefficients are given by

$$v_n(p_T) = \frac{\int_0^{2\pi} d\phi\, f(p_T,\phi)\, \cos(n\phi)}{\int_0^{2\pi} d\phi\, f(p_T,\phi)} \tag{54}$$

with[46]

$$f(p_T,\phi) \equiv f_{(+x)}(p_T,\phi,y=0) + f_{(-x)}(p_T,\phi,y=0) + f_{(+y)}(p_T,\phi,y=0) + f_{(-y)}(p_T,\phi,y=0)\ . \tag{55}$$

For each source we take viscous corrections of the Grad form (42) with uniform shear stress across the fireball, where $\pi^{\mu\nu}$ is a boosted copy of the 0+1D Bjorken shear stress solution (41). This way, the dimensionless $\kappa \equiv \pi_L/(e+p)$ is our only extra parameter, and it is the same for all four fireballs. Note that for typical viscous 0+1D Bjorken evolution $\kappa < 0$ because the longitudinal shear stress is negative (see [16] for an extensive analysis). Setting $\kappa = 0$ reproduces the ideal fluid results in [32].

Straightforward calculation yields anisotropic flow coefficients in terms of modified Bessel functions of the first kind (see App. F for details). Here we only discuss v_2 but in general all even v_n are nonzero. From (F7),

$$v_2(p_T) = \frac{G_2(a_x,b_x,z,c\kappa) - G_2(a_y,b_y,z,c\kappa)}{G_0(a_x,b_x,z,c\kappa) + G_0(a_y,b_y,z,c\kappa)}\ , \tag{56}$$

where

$$z \equiv \frac{m}{T}\ , \quad a_i \equiv \frac{\sqrt{m^2+p_T^2}}{T\sqrt{1-v_i^2}}\ , \quad b_i \equiv \frac{v_i p_T}{T\sqrt{1-v_i^2}} \qquad (i=x,y)\ , \tag{57}$$

c is the magnitude of the viscous correction *relative* to the "democratic" Grad case, and G_n is given by (F8). Figure 4 shows the result for $T = 140$ MeV, $v_x = 0.5$, $v_y = 0.45$, with $\kappa = -0.06$ which corresponds to $\pi_L/p \approx -0.4$ (at this temperature $e/p \approx 5.5$). The local thermal equilibrium curves (filled circles) exhibit the well-known mass ordering of ellipit flow (see [32] for more discussion). Relative to this baseline, viscous corrections reduce elliptic flow for both protons and pions. The reduction for protons, however, is only half as large from the self-consistent approach (crosses) compared to the "democratic" Grad ansatz (open boxes). Though this simple model does not capture the flattening of v_2 at $p_T \gtrsim 1.5$ GeV in Fig. 3, it does illustrate that viscous corrections generally make elliptic flow smaller.

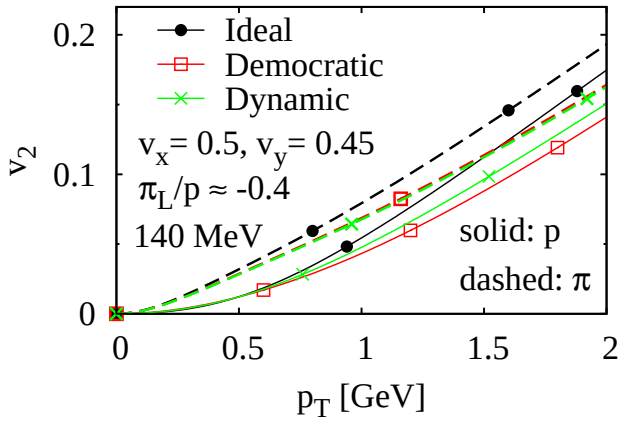

FIG. 4: Differential elliptic flow $v_2(p_T)$ from a viscous generalization of the simple four-source model of Ref. [32] with parameters $v_x = 0.5$, $v_y = 0.45$, $T = 140$ MeV, and $\kappa \equiv \pi_L/(e+p) = -0.06$. Dashed lines are for pions, while solid curves are for protons. The standard "democratic Grad" approach (open boxes, $c_\pi = c_p = 1$) is compared to self-consistent shear corrections (crosses, $c_\pi = 1.03$ and $c_p = 0.55$) computed for a pion-nucleon gas from linearized kinetic theory (see Sec. IV B). Results with uncorrected, local equilibrium phase space distributions ($c_\pi = c_p = 0$) are also shown (filled circles).

V. MULTICOMPONENT HADRON GAS

In Section IV B self-consistent corrections were calculated for a pion-nucleon gas. This is clearly an estimate only because it ignores interactions of pions and nucleons with other species in the system. It is natural to extend the investigation to mixtures with many hadronic species, in which case each species will have its own dissipative corrections based on the microscopic dynamics. The problem is complicated, however, because it requires knowledge of hadronic scattering rates between all species. In principle these are encoded in hadron transport codes, such as UrQMD[27], AMPT[28], or JAM[29], and we plan to apply these in a future study. Here we only pursue two simple models: i) a hadron gas with the same, fixed scattering cross section for all species, which is the model in Ref. [30]; and ii) a gas with more realistic cross sections that follow additive quark model[27, 31] (AQM) scaling, i.e., constant meson-meson, meson-baryon, and baryon-baryon cross sections with ratios $\sigma_{MM} : \sigma_{MB} : \sigma_{BB} = 4 : 6 : 9$. In both cases we only consider elastic $ij \to ij$ channels (allowing for $i = j$), with energy-independent, isotropic cross sections.

For the fixed cross section scenario we use $\sigma_{ij} = 30$ mb, the same value as the effective $\sigma_{\pi\pi}$ for the pion-nucleon gas earlier (cf. Fig. 3). For the AQM model, we take $\sigma_{MM} = 30$ mb, which implies $\sigma_{MB} = 45$ mb, and $\sigma_{BB} = 67.5$ mb. To simplify the computation, we combine, as in Section IV B, members of the same isospin multiplet, and their antiparticle partners as well, into a single species with appropriately scaled degeneracy so that the number of degrees of freedom and particle densities stay the same. The following calculation includes hadrons up to $m = 1.672$ GeV, i.e., the $\Omega(1672)$, which translates into 49 effective species (the c_i coefficients for the 49 species in the various scenarios are listed in Appendix G).

A. Elliptic flow for mixture in Grad approximation

Figure 5 shows pion and proton elliptic flow $v_2(p_T)$ in $Au + Au$ at RHIC at $b = 7$ fm from a calculation analogous to the $\pi - N$ system in Section IV B with Cooper-Frye particle conversion applied at $T_{conv} = 165$ MeV, except now with self-consistent phase space corrections δf_i calculated for the multicomponent hadron gas. The left plot is for $\sigma_{ij} = const$, in which case pion and proton elliptic flow are very close to results from the "democratic" approach. The lack of species dependence is very similar to the findings of Ref. [30]. If one looks closely, however, at high p_T, proton flow is actually slightly higher than pion flow, reflecting the decrease in shear stress corrections with mass at fixed cross section (cf. Section IV).

The right plot of Fig. 5 shows, on the other hand, that more realistic additive quark model cross sections do generate a pion-proton difference in elliptic flow, of similar magnitude to the difference seen for a pion-nucleon gas earlier. Crossing between pion and proton v_2 also happens at about the same $p_T \sim 1$ GeV. The likely explanation for this is that even though interactions with all species are now considered, interactions with pions dominate because

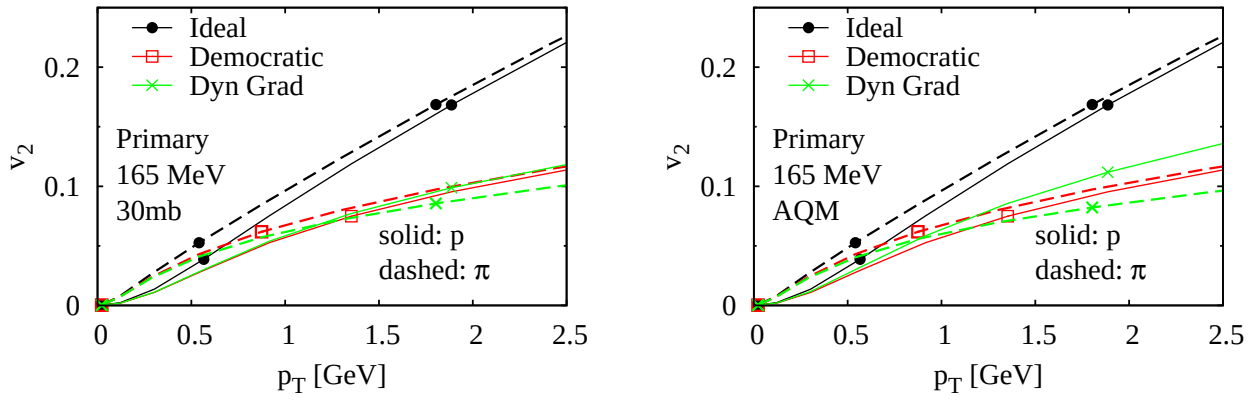

FIG. 5: Same as Fig. 3, except the self-consistent viscous corrections are computed for a gas of all hadron species up to m=1.672 GeV ($\Omega(1672)$), with members of each isospin multiplet (and antiparticles) combined together into a single effective species. There are 49 effective species this way. *Left plot:* all hadron species interacting with the same constant isotropic cross section $\sigma_{ij} = 30$ mb. *Right plot:* constant isotropic cross sections with additive quark model scaling $\sigma_{MM} : \sigma_{MB} : \sigma_{BB} = 4 : 6 : 9$ and $\sigma_{MM} = 30$ mb. Calculations with the "democratic Grad" ansatz for $\eta_s/s = 0.1$ (open boxes) and with local equilibrium distribution (filled circles) are also shown. In all cases, and for both plots, the Cooper-Frye prescription is applied at $T_{conv} = 165$ MeV.

at $T_{conv} = 165$ MeV pions have a much higher density compared to all other species, including kaons, the second lightest species. Though not shown here, we note that for $T_{conv} = 140$ MeV one finds the same: the fixed cross section scenario closely matches the "democratic" Grad results, whereas pion-proton splitting in the AQM scenario is very similar in magnitude to the $T_{conv} = 140$ MeV result of Fig. 3 (right plot).

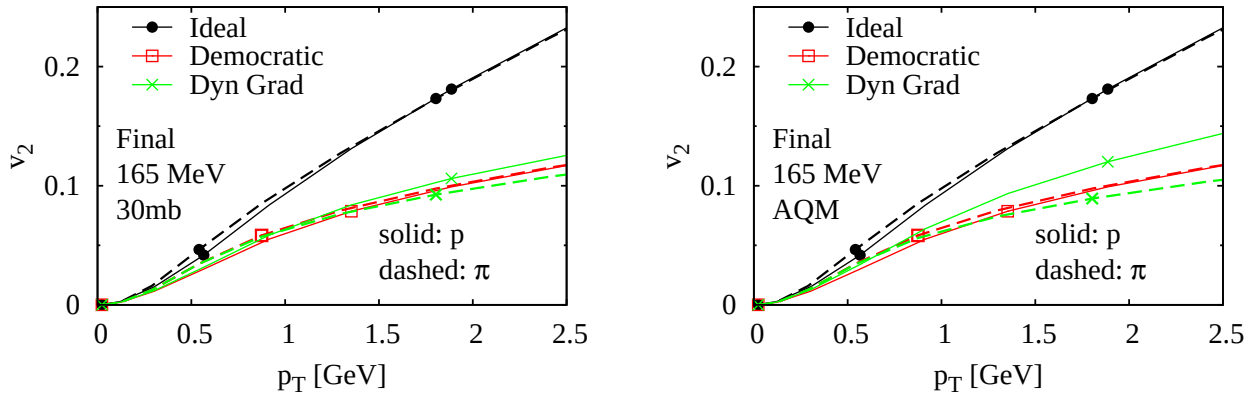

FIG. 6: Same as Fig. 5, except after feeddown from resonance decays using the RESO code in the AZHYDRO package[22].

The Cooper-Frye prescription gives the momentum distribution of particles emitted directly from the fluid ("primary" particles). In a pure hydrodynamic approach, i.e., without a hadronic afterburner, many of these particles later decay en route to the detectors. Figure 6 shows the p_T dependence of pion and proton elliptic flow from the same calculation shown in Fig. 5, except unstable resonances are decayed using the RESO code in the AZHYDRO package[22] (stable hadrons in RESO are the pions, kaons, and nucleons). For ideal freezeout ($\delta f = 0$), the "democratic Grad" ansatz, and also the constant cross section scenario, the main effect of resonance decays on elliptic flow is a reduction of the pion-proton splitting at low p_T, while at high p_T there is barely any effect. For all three scenarios, at $T_{conv} = 165$ MeV the difference between pions and protons for all three scenarios gets washed out almost completely (this is not universal at all temperatures, for lower $T_{conv} = 140$ or 120 MeV, a portion of the difference survives). In contrast, in the more realistic AQM scenario, with self-consistent viscous fluid-to-particle conversion, proton elliptic flow stays 30% higher at $p_T \sim 2$ GeV than pion elliptic flow even after resonance decays are taken into account. The

TABLE III: Variational maxima of the functional $Q[\chi]$ as a function of temperature for a mixture of hadrons up to $m = 1.672$ GeV, with power law variational ansatz $\delta f_i \propto p^\alpha$, and zero chemical potentials, for constant cross sections $\sigma_{ij} = 30$ mb. All values are rounded to the two most significant digits.

$\delta f/f^{eq}$	T=100	120	140	165 MeV
$\propto p^1$ (linear)	1.10	0.79	0.60	0.45
$\propto p^{3/2}$	1.16	0.83	0.63	0.47
$\propto p^2$ (Grad)	1.12	0.80	0.61	0.45

TABLE IV: Variational maxima of the functional $Q[\chi]$ as a function of temperature for a mixture of hadrons up to $m = 1.672$ GeV, with power law variational ansatz $\delta f_i \propto p^\alpha$, and zero chemical potentials, for additive quark model[31] (AQM) cross sections with $\sigma_{MM} = 30$ mb (see text). All values are rounded to the two most significant digits.

$\delta f/f^{eq}$	T=100	120	140	165 MeV
$\propto p^1$ (linear)	1.09	0.76	0.55	0.39
$\propto p^{3/2}$	1.15	0.80	0.58	0.41
$\propto p^2$ (Grad)	1.10	0.77	0.56	0.39

same insensitivity to resonance decays is present at $T_{conv} = 140$ MeV and 120 MeV as well (not shown).

B. Elliptic flow for mixture with $\delta f \propto p$ or $p^{3/2}$

Finally to investigate systematic errors due to the assumed quadratic momentum dependence of dissipative corrections (Grad ansatz), we explore instead power law momentum dependence with $\delta f_i/f_i^{\rm eq} \propto p$ and $p^{3/2}$. These correspond to (23) with

$$\chi_i^{(1)}(|\tilde{\mathbf{p}}|) = c_i|\tilde{\mathbf{p}}|^{-1} \quad , \qquad \chi_i^{(3/2)}(|\tilde{\mathbf{p}}|) = c_i|\tilde{\mathbf{p}}|^{-1/2} \qquad (\chi_i^{Grad} = c_i|\tilde{\mathbf{p}}|^0) \ , \tag{58}$$

where coefficients are determined variationally via maximizing $Q[\chi]$ and thus, in general, they vary among species. These choices are motivated by earlier studies that found $p^{3/2}$ dependence for a mixture of massless quarks and gluons with small-angle $1 \leftrightarrow 2$ interactions[6], and also close to $p^{3/2}$ dependence for single-component and two-component systems of massless particles with energy-independent, isotropic $2 \to 2$ cross sections[5]. The two new forms here have weaker momentum dependence than the quadratic Grad correction, therefore at high p_T they will in general exhibit smaller dissipative effects than the dynamical Grad results. For example, elliptic flow is less suppressed at high p_T.

Figures 7 and 8 show pion and proton elliptic flow as a function of p_T for the gas of hadrons up to $m = 1.672$ GeV with fluid-to-particle conversion at $T_{conv} = 165$ MeV using self-consistent linear $\delta f_i \propto p$, and $\delta f_i \propto p^{3/2}$, respectively. For both figures, feeddown from resonance decays is included. For the constant cross section scenario (left plots), pions and protons have basically the same v_2, and the main effect is an overall increase in v_2 at high p_T by nearly 20% and 40% for $p^{3/2}$ and p^1 momentum dependence, respectively, relative to the common "democratic Grad" approach. For the more realistic AQM scenario, we see a narrowing of the separation between pion and proton v_2 as the power n increases in $\delta f \propto p^n$. At the same time, v_2 increases for both species. With self consistent fluid-to-particle conversion the viscous suppression of proton elliptic flow is nearly two times smaller for $\delta f \propto p^{3/2}$, and slightly more than two times smaller for $\delta f \propto p$, relative to the democratic approach,

One can check which of the three powers is most consistent, variationally, with the underlying microscopic dynamics by looking at the maximum value of Q. As shown in Tables III-IV, in the entire temperature range $100 < T_{conv} < 165$ MeV we studied, $p^{3/2}$ dependence is favored compared to both linear and quadratic momentum dependence in δf. This should provide impetus for using $\delta f \propto p^{3/2}$ dependence instead of the common quadratic ansatz in fluid dynamical calculations and hybrid models. However, the results here underscore the need for species-dependent viscous corrections even in that case.

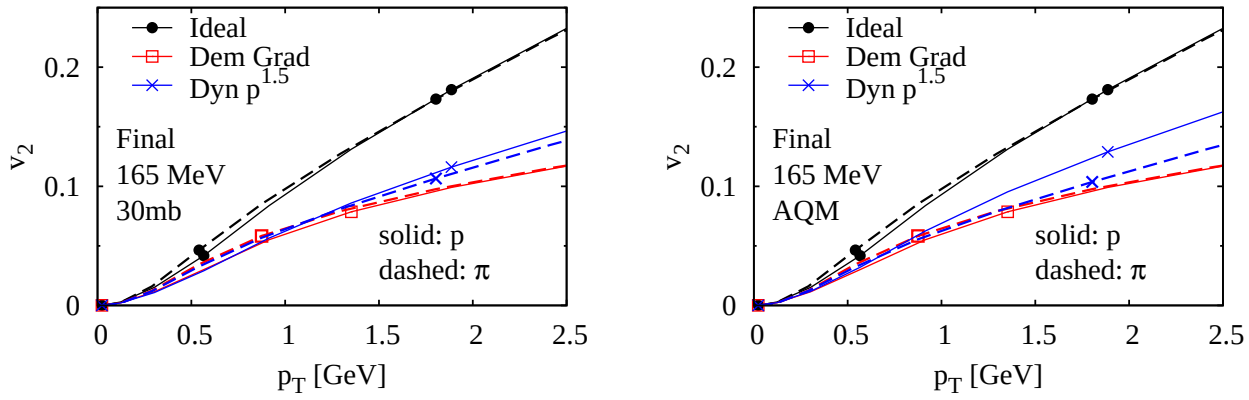

FIG. 7: Differential elliptic flow $v_2(p_T)$ for pions and protons in $Au+Au$ at $\sqrt{s_{NN}} = 200$ GeV at RHIC with impact parameter $b = 7$ fm, using 2+1D boost invariant hydrodynamic solutions from AZHYDRO[21, 22], followed by Cooper-Frye fluid-to-particle conversion at $T_{conv} = 165$ MeV with either the standard "democratic" approach (open boxes) or self-consistent shear corrections (crosses) with momentum dependence $\delta f \propto p^{3/2}$ computed from kinetic theory for a gas of hadrons up to $m = 1.672$ GeV. In both plots, dashed lines are for pions, while solid curves are for protons, and feeddown from resonance decays is included. *Left plot:* scenario with constant 30-mb hadronic cross sections. *Right plot:* cross sections based on the additive quark model (AQM). Results with uncorrected, local equilibrium phase space distributions ($\delta f = 0$) are also shown (filled circles).

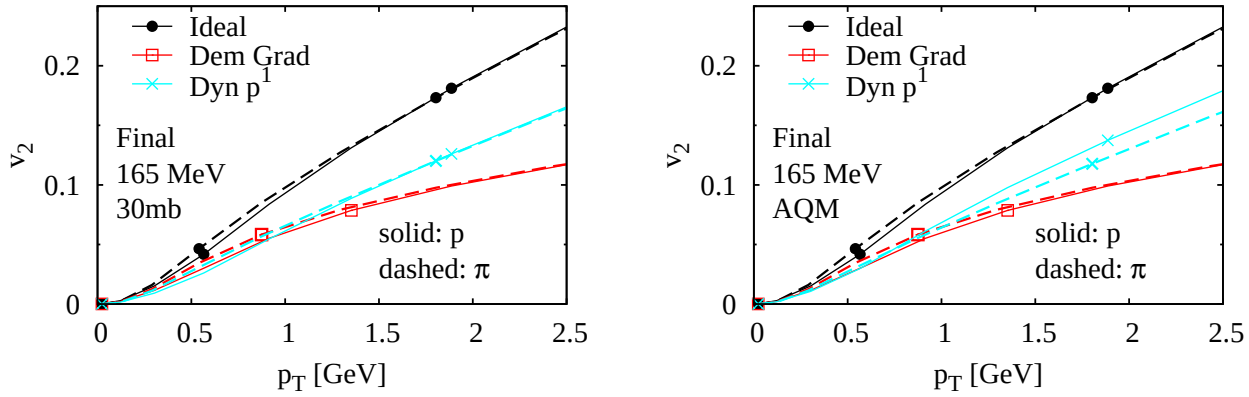

FIG. 8: Same as Fig. 7, except with momentum dependence $\delta f \propto p$ for the curves from self-consistent fluid-to-particle conversion (crosses).

C. Sensitivity to shear viscosity

The results in Secs. V A and V B correspond to a fixed set of values for hadronic cross sections, or equivalently, a fixed shear viscosity to entropy density ratio $\eta_s/s = 0.1$. In Fig. 9 we explore the sensitivity of differential elliptic flow $v_2(p_T)$ in $Au+Au$ at RHIC to η_s/s for both p^2 (Grad) and $p^{3/2}$ viscous corrections in the additive quark model (AQM) scenario. All parameters are the same as in Figs. 6 and 7, except the bands plotted for pions and protons correspond to $0.05 \leq \eta_s/s \leq 0.15$ (σ_{MM} is varied between 20 and 60 mb, and all hadronic cross sections are scaled up and down proportionally). The magnitude of viscous corrections in $v_2(p_T)$ relative to the ideal (nonviscous) case, of course, varies with η_s/s. In fact, the dependence on η_s/s is monotonic, with the top of the bands always corresponding to the lowest value $\eta_s/s = 0.05$. Still, the pion-proton splitting in $v_2(p_T)$ due to the self-consistent viscous corrections is present at all η_s/s values, and the relative difference between pion and proton viscous corrections stays roughly the same.

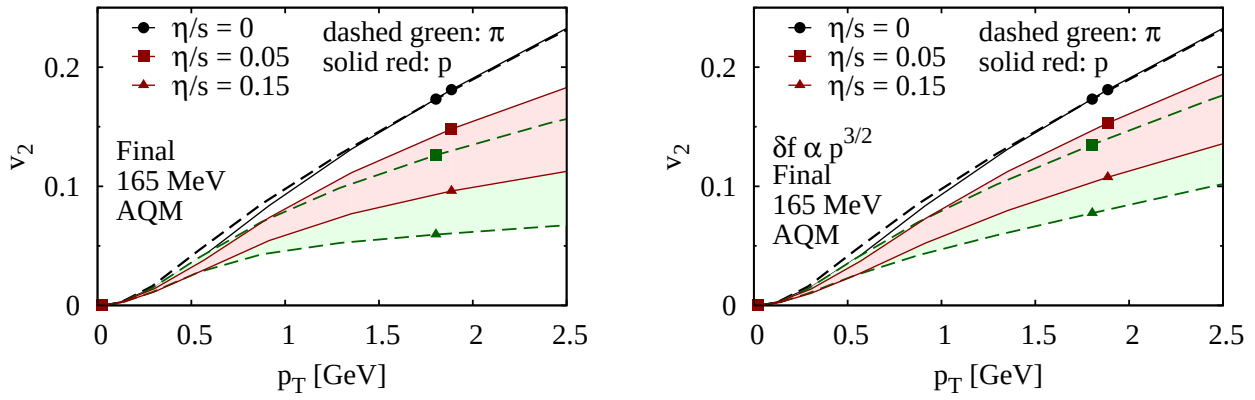

FIG. 9: Same as the right plots in Figs. 6 and 7 for $Au + Au$ at RHIC with self-consistent viscous corrections in the additive quark model (AQM) scenario with $\delta f \propto p^2$ (left) and $\delta f \propto p^{3/2}$ (right) but with η_s/s varied in the range $0.05 \leq \eta_s/s \leq 0.15$. Shaded bands are shown together with curves at the lowest $\eta_s/s = 0.05$ (squares) and highest $\eta_s/s = 0.15$ (triangles) boundaries.

VI. CONCLUSIONS

Reliable extraction of medium properties from heavy-ion data using hydrodynamics or hybrid hydrodynamics+transport models inevitably requires conversion of a dissipative fluid to particles (hadrons). The popular approach is to apply the Cooper-Frye formula (E2) with hadron phase space densities $f_i = f_i^{eq} + \delta f_i$ that include nonequilibrium corrections of quadratic form in momentum with a universal species independent coefficient ("democratic Grad" ansatz). This simple scheme ignores the dynamics of equilibration in the hadron gas. In this work we obtain instead self-consistent shear viscous corrections from linearized kinetic theory (Section II). This approach in general gives species-dependent phase space corrections δf_i, which are then reflected in identified particle observables. The effect on identified particle elliptic flow is demonstrated in Section V.

Phenomenological applications are necessarily numerical because of the many species involved. But to aid with interpretation we discuss extensively analytic and numerical results for massless and massive two-component systems in Sections III and IV. We also provide a comparison to fully nonlinear covariant transport to justify the approach.

Several simplifications are made in this work, which will be improved in future publications. For example, realistic energy-dependent hadronic cross sections and realistic viscous hydrodynamic evolution will, of course, have to be included. The momentum dependence of viscous corrections $\delta f_i/f_i^{eq}$ is also simplified here to quadratic or power-law form in momentum. Nevertheless, it would be very interesting to check how the self-consistent viscous distributions obtained here influence observables from hydrodynamic and hybrid models, and the interpretation of heavy-ion data. To aid this we provide scaling factors in Appendix G that can be used to "patch" the commonly used democratic approach with the species-dependent viscous corrections calculated in this work.

Acknowledgments

Insightful discussions with Gabriel Denicol, Derek Teaney, Guy Moore, Sangyong Jeon, and Raju Venugopalan are acknowledged. D.M. thanks RIKEN, Brookhaven National Laboratory and the US Department of Energy for providing facilities essential for the completion of this work. D.M. also thanks the hospitality of the Wigner Research Center for Physics (Budapest, Hungary), and the Institute for Nuclear Theory (Seattle, Washington), where parts of this work have been done. Computing resources managed by RCAC/Purdue are also gratefully acknowledged. This work was supported by the U.S. Department of Energy, Office of Science, under grants DE-AC02-98CH10886 [RIKEN BNL] and DE-PS02-09ER41665.

Appendix A: General form of ϕ

The form (23) comes from expanding $\phi_i(x,\mathbf{p})$ in terms of irreducible tensors[33]

$$\phi_i(x,\mathbf{p}) = \sum_{r=0}^{\infty} a_r(|\tilde{\mathbf{p}}|)\, P^{(r)}(p)\cdot X^{(r)}(x)\ , \tag{A1}$$

which is just a Lorentz covariant way to write an expansion over spherical harmonics in the LR frame (the $(\cdot)$ denotes full contraction of tensors $P^{(r)}$ and $X^{(r)}$). $P^{(r)}$ is a rank-r irreducible tensor projected out from the fully symmetric, rank-r Lorentz tensor $p^{\mu_1}p^{\mu_2}\cdots p^{\mu_r}$ such that $P^{(r)}$ is purely spatial in the LR frame (orthogonal to u in any index) and vanishes under contraction of any two of its indices, so it is the irreducible representation with maximal angular momentum r from the tensor product of r three-dimensional (spin-1) vectors in the LR frame, $\overbrace{\tilde{\mathbf{p}}\otimes\tilde{\mathbf{p}}\otimes\cdots\otimes\tilde{\mathbf{p}}}^{r}$. For example, with suitable normalization, $P^{(2)}_{\mu\nu}(p) = P_{\mu\nu}$ defined in (21). Because ϕ_i is a Lorentz scalar, $X^{(r)}$ is also a rank-r irreducible tensor, while the coefficients a_r are invariant under rotations in the LR frame, so their momentum dependence is only through the LR-frame particle energy, or equivalently, the normalized momentum magnitude $|\tilde{\mathbf{p}}|$. The expansion (A1) can be inverted for $X^{(r)}$ through integration using the orthogonality of invariant tensors:

$$X^{(r)}(x) \propto \int \frac{d^3p}{E} P^{(r)}(p)\phi_i(x,\mathbf{p})\ , \tag{A2}$$

where the omitted proportionality constant depends on $|\tilde{\mathbf{p}}|$. Inverting both sides of (20), the shear source term (22) only contributes for $r=2$, and the result is proportional to $X^{\mu\nu}$, so the RHS must give a similar contribution only for $r=2$. Because the linearized collision operator commutes with Lorentz transformations, contains scalar functions of momentum, and $f_i^{\rm eq}$ only depends on $|\tilde{\mathbf{p}}|$, the collision operator preserves the expansion (A1) except for the coefficients a_r. Thus, (23) indeed follows.

Appendix B: Calculation of momentum integrals in $\boldsymbol{Q}[\boldsymbol{\chi}]$

All required integrals are scalars, so it is convenient to integrate momenta 3 and 4 in the center-of-mass (CM) of the scattering process (momentum conservation is simpler), while momenta 1 and 2 in the LR frame of the fluid (so that $f^{\rm eq}\propto e^{-E/T}$ is isotropic). For brevity, in this entire Section *LR* subscripts are omitted, while *CM* variables are distinguished with an overbar wherever confusion might arise. Spherical coordinates are also helpful.

B_1 can be reduced to one dimensional integration, Q_{11} and Q_{22} to three dimensions, while Q_{31} and Q_{41} to five dimensions in general, or four in the case of isotropic cross sections. All remaining integrals were performed numerically using adaptive integration routines from the GNU Scientific Library (GSL) [34].

1. Reduction of terms B, Q_{11}, and Q_{21}

The source term B_i in (28), which is linear in χ_i, immediately reduces this way to

$$B_i = \frac{2\pi}{3T^6}\int_{m_i}^{\infty} dE_1\, p_1^5 f_{1i}^{\rm eq}\chi_{1i}\ . \tag{B1}$$

In the terms quadratic in χ, $\bar{\mathbf{p}}_4$ can be eliminated using the δ-function in three-momentum, and the magnitude of $|\bar{\mathbf{p}}_3|$ is set by the δ-function in energy:

$$\iint_{3\,4}\delta^4(12-34)\ (...) = \frac{1}{4}\int d\bar{\Omega}_3 d\bar{p}_3 \frac{\bar{p}_3^2}{\bar{E}_3\bar{E}_4}\delta(\bar{E}_3+\bar{E}_4-\sqrt{s})\ (...) = \left.\frac{p'_{cm}}{4\sqrt{s}}\int d\bar{\Omega}_3\ (...)\right|_{\bar{p}_3=p'_{cm}}\ . \tag{B2}$$

For the χ_{1i}^2 and $\chi_{1i}\,\chi_{2j}$ terms one can substitute (16) to obtain

$$\int_{34}\delta^4(12-34)\bar{W}^{ij\to k\ell}_{12\to 34} = p_{cm}\sqrt{s}\,(1+\delta_{k\ell})\,\sigma_{TOT}^{ij\to k\ell}(s)\ , \tag{B3}$$

and the calculation is then analogous to the scattering rate in Appendix C. Keeping $t_{12} \equiv \cos\theta_{12}$, one has

$$Q_{11}^{ij\to k\ell} = \frac{2\pi^2}{3T^8}(1+\delta_{k\ell}) \int\limits_{m_i}^{\infty} dE_1\, p_1^5\, f_{1i}^{\rm eq}\, \chi_{1i}^2 \int\limits_{m_j}^{\infty} dE_2\, p_2\, f_{2j}^{\rm eq} \int\limits_{-1}^{1} dt_{12}\, F(s)\, \sigma_{TOT}^{ij\to k\ell}(s) \tag{B4}$$

and

$$Q_{21}^{ij\to k\ell} = \frac{\pi^2}{3T^8}(1+\delta_{k\ell}) \int\limits_{m_i}^{\infty} dE_1\, p_1^3\, f_{1i}^{\rm eq}\, \chi_{1i} \int\limits_{m_j}^{\infty} dE_2\, p_2^3\, f_{2j}^{\rm eq}\, \chi_{2j} \int\limits_{-1}^{1} dt_{12}\, (3t_{12}^2-1)\, F(s)\, \sigma_{TOT}^{ij\to k\ell}(s)\ , \tag{B5}$$

where F is given by (52).

2. Reduction of terms Q_{31} and Q_{41}

The last two $\chi_1\chi_3$ and $\chi_1\chi_4$ terms in general involve numerical integration in 9-4=5 dimensions (three momentum integrals with a 4D δ-function constraint) because χ_3 and χ_4 depend on outgoing three-momenta in the LR frame. Interchange symmetry (14) with $3 \leftrightarrow 4$, $k \leftrightarrow \ell$ implies $Q_{41}^{ij\to k\ell} = Q_{31}^{ij\to \ell k}$, so it is enough to discuss Q_{31}. For isotropic cross section, it is possible to do one more integral analytically, if the LR frame momentum $\mathbf{p}_3$ is expressed using the CM frame momentum $\bar{\mathbf{p}}_3 \equiv p'_{cm}\bar{\mathbf{n}}_3$ (here $|\bar{\mathbf{n}}_3| = 1$). Lorentz boost from CM to LR gives

$$E_3 = \gamma_3 E_T + \beta_3 \mathbf{p}_T \bar{\mathbf{n}}_3\ , \qquad \mathbf{p}_3 = p'_{cm}\bar{\mathbf{n}}_3 + \mathbf{p}_T \left(\gamma_3 + \beta_3 \frac{\mathbf{p}_T\bar{\mathbf{n}}_3}{E_T+\sqrt{s}}\right)\ , \tag{B6}$$

where

$$\beta_3 \equiv \frac{p'_{cm}}{\sqrt{s}} \quad , \qquad \gamma_3 \equiv \frac{\bar{E}_3}{\sqrt{s}} = \sqrt{\beta_3^2 + \frac{m_k^2}{s}} \quad , \qquad E_T \equiv E_1 + E_2 \quad , \qquad \mathbf{p}_T \equiv \mathbf{p}_1 + \mathbf{p}_2 \tag{B7}$$

only depend on $\mathbf{p}_1$ and $\mathbf{p}_2$ but not on $\bar{\mathbf{p}}_3$. With convenient angles $\bar{\mathbf{n}}_3(\phi_3, \theta_3)$ for the $d\bar{\Omega}_3$ integration such that the zenith direction is parallel to $\mathbf{p}_T$,

$$\bar{\mathbf{n}}_3\mathbf{p}_T = p_T\cos\theta_3\ , \qquad \bar{\mathbf{n}}_3\mathbf{p}_1 = p_1(\sin\theta_1\sin\theta_3\cos\phi_3 + \cos\theta_1\cos\theta_3)\ , \tag{B8}$$

where

$$\cos\theta_1 \equiv \frac{\mathbf{p}_T\mathbf{p}_1}{p_T p_1} = \frac{p_1 + p_2 t_{12}}{p_T}\ . \tag{B9}$$

Because $|\bar{\mathbf{p}}_3|$ does not depend on ϕ_3, the only ϕ_3 dependence is in the $(\mathbf{p}_3\mathbf{p}_1)^2$ term from $P_3 \cdot P_1$, which can be integrated. So even if the total cross section depends on energy, we have only four integrals remaining:

$$\iint\limits_{1\,2}\int d\Omega_3\,(...) = \frac{4\pi\cdot 2\pi\cdot 2\pi}{4} \int\limits_{m_i}^{\infty} dE_1\, p_1 \int\limits_{m_j}^{\infty} dE_2\, p_2 \int\limits_{-1}^{1} dt_{12} \int\limits_{-1}^{1} dt_3\, \langle(...)\rangle_{\phi_3} \tag{B10}$$

i.e.,

$$Q_{31}^{ij\to k\ell} = \frac{\pi^2}{2T^8}(1+\delta_{k\ell}) \int\limits_{m_i}^{\infty} dE_1\, p_1\, f_{1i}^{\rm eq}\, \chi_{1i} \int\limits_{m_j}^{\infty} dE_2\, p_2\, f_{2j}^{\rm eq} \int\limits_{-1}^{1} dt_{12} F(s) \sigma_{TOT}^{ij\to k\ell}(s) \int\limits_{-1}^{1} dt_3\, \chi_{3k}\, \langle P_3\cdot P_1\rangle_{\phi_3}\ , \tag{B11}$$

where $t_3 \equiv \cos\theta_3$, $p_3 = |\mathbf{p}_3| = \sqrt{(\gamma_3 E_T + \beta_3 p_T t_3)^2 - m_k^2}$, and

$$\langle(...)\rangle_{\phi_3} \equiv \frac{1}{2\pi}\int\limits_0^{2\pi} d\phi_3 (...) \tag{B12}$$

denotes averaging over ϕ_3. The following ϕ_3 averages appear:

$$\langle \bar{\mathbf{n}}_3 \mathbf{p}_1 \rangle_{\phi_3} = p_1 \cos\theta_1 t_3 \quad , \qquad \langle (\bar{\mathbf{n}}_3 \mathbf{p}_1)^2 \rangle_{\phi_3} = \frac{p_1^2}{2}[(3t_3^2 - 1)\cos^2\theta_1 + 1 - t_3^2] \ , \tag{B13}$$

in terms of which

$$\begin{aligned} \langle P_3 \cdot P_1 \rangle_{\phi_3} \ = \ & \frac{1}{T^4} \left[(p'_{cm})^2 \langle (\bar{\mathbf{n}}_3 \mathbf{p}_1)^2 \rangle_\phi + p_1^2 (p_1 + p_2 t_{12})^2 \left(\gamma_3 + \beta_3 \frac{p_T t_3}{E_1 + E_2 + \sqrt{s}} \right)^2 \right. \\ & \left. + \ 2 p'_{cm} p_1 (p_1 + p_2 t_{12}) \left(\gamma_3 + \beta_3 \frac{p_T t_3}{E_1 + E_2 + \sqrt{s}} \right) \langle \bar{\mathbf{n}}_3 \mathbf{p}_1 \rangle_\phi \right] - \frac{p_1^2 p_3^2}{3T^4} \end{aligned} \tag{B14}$$

3. Integration using auxiliary variable ω

The method outlined above is practical but limited to isotropic cross section. For general $d\sigma(s,t)/dt$, one can evaluate Q_{31} and Q_{41} via extending the technique used in Ref. [15] to massive particles. The key elements of that technique are splitting the energy conservation integral with the help the energy transfer ω as

$$\delta(E_1 + E_2 - E_3 - E_4) \equiv \int\limits_{-\infty}^{\infty} \delta(\omega + E_1 - E_3)\, \delta(\omega - E_2 + E_4) \ , \tag{B15}$$

eliminating $\mathbf{p}_4$ through momentum conservation, and swapping $\mathbf{p}_3$ for the momentum transfer $\mathbf{q} \equiv \mathbf{p}_3 - \mathbf{p}_1$. Exploiting rotation invariance, introduce angles such that

$$\mathbf{q} = q(0,0,1) \ , \quad \mathbf{p}_1 = p_1(\sin\theta_{1q}, 0, \cos\theta_{1q}) \ , \quad \mathbf{p}_2 = p_2(\cos\phi \sin\theta_{2q}, \sin\phi \sin\theta_{2q}, \cos\theta_{2q}) \ . \tag{B16}$$

Then the Mandelstam variables for the scattering process are

$$s = m_i^2 + m_j^2 + 2(E_1 E_2 - \mathbf{p}_1 \mathbf{p}_2) \quad , \qquad t = \omega^2 - q^2 \ , \tag{B17}$$

the magnitudes of outgoing momenta are

$$p_3 = \sqrt{(E_1 + \omega)^2 - m_k^2} \ , \quad p_4 = \sqrt{(E_2 - \omega)^2 - m_\ell^2} \ , \tag{B18}$$

and the scalar products that appear in s and $P \cdot P$ are

$$\begin{aligned} & \mathbf{p}_1 \mathbf{p}_2 = p_1 p_2 (\cos\theta_{1q} \cos\theta_{2q} + \cos\phi \sin\theta_{1q} \sin\theta_{2q}) \ , \qquad \mathbf{p}_1 \mathbf{p}_3 = p_1^2 + \frac{m_i^2 - m_k^2 + 2E_1\omega + t}{2} \ , \\ & \mathbf{p}_1 \mathbf{p}_4 = p_1^2 + \mathbf{p}_1 \mathbf{p}_2 - \mathbf{p}_1 \mathbf{p}_3 \ , \end{aligned} \tag{B19}$$

where the θ angles are fixed by the δ-functions:

$$\cos\theta_{1q} = \frac{m_i^2 - m_k^2 + 2E_1\omega + t}{2p_1 q} \ , \qquad \cos\theta_{2q} = \frac{m_\ell^2 - m_j^2 + 2E_2\omega - t}{2p_2 q} \ . \tag{B20}$$

Five integrals remain:

$$\iiiint\limits_{1234} \delta^4(12-34)\ (...) = \frac{\pi^2}{2} \int\limits_{m_1}^{\infty} dE_1 \int\limits_{m_2}^{\infty} dE_2 \int\limits_0^{2\pi} d\phi \int\limits_0^{\infty} dq \int\limits_{-\infty}^{\infty} d\omega\, \Theta(1 - \cos^2\theta_{1q})\, \Theta(1 - \cos^2\theta_{2q})(...) \ , \tag{B21}$$

where the Heaviside functions set the integration limits.

For equal masses $m_i = m_j = m_k = m_\ell \equiv m$,

$$\iiiint\limits_{1234} \delta^4(12-34)\ (...) = \frac{\pi^2}{2} \int\limits_0^{\infty} dq \int\limits_{-q}^{q} d\omega \int\limits_{\bar{\Lambda}(q,-\omega)}^{\infty} dE_1 \int\limits_{\bar{\Lambda}(q,\omega)}^{\infty} dE_2 \int\limits_0^{2\pi} d\phi\ (...) \ , \tag{B22}$$

where

$$\bar{\Lambda}(q,\omega) = \sqrt{m^2 + \Lambda^2(q,\omega)} \quad , \qquad \Lambda(q,\omega) = \left| \frac{q + \omega\sqrt{1 - \frac{4m^2}{t}}}{2} \right| \ , \tag{B23}$$

and we verified that both methods give numerically identical results with isotropic cross sections. The main disadvantage compared to the method in the previous Subsection is speed - for isotropic cross section one still has five numerical integrals to do compared to four in (B11).

Appendix C: Evaluation of scattering rates

The scattering rate integral (51) right away reduces from six dimensions to only three because in the static case the phase space density $f^{\rm eq} \propto e^{-E/T}$ and Mandelstam

$$s \equiv m_i^2 + m_j^2 + 2(E_1 E_2 - \mathbf{p}_1\mathbf{p}_2) \tag{C1}$$

only depend on the magnitudes of momenta and the angle θ_{12} between them. Replacing $\cos\theta_{12}$ with s, in spherical coordinates we then have

$$\int \frac{d^3p_1}{E_1}\frac{d^3p_2}{E_2}(...) = 4\pi\cdot 2\pi \int\limits_{m_i}^{\infty} dE_1 \int\limits_{m_j}^{\infty} dE_2 \int\limits_{s_-}^{s_+} ds\,(...) \tag{C2}$$

with limits $s_\pm = m_i^2 + m_j^2 + 2\left[E_1E_2 \pm \sqrt{(E_1^2 - m_i^2)(E_2^2 - m_j^2)}\right]$.

Though not pursued here, further simplification of the $2 \to 2$ scattering rate is possible. If speed of evaluation is a concern, consult Appendix A of Ref. [35] (integrated rate for equal mass particles), Appendix B of Ref. [36] (rate for fixed particle momentum), or Ref. [37] (integrated rate for arbitrary masses).

Appendix D: Grad results in nonrelativistic limit

In the nonrelativistic limit one can replace terms in (B4), (B5), and (B11) with their nonrelativistic counterparts

$$\frac{d^3p}{E} \to \frac{d^3p}{m} \ , \quad dE \to \frac{dp\,p}{m} \ , \quad \exp\!\left(-\frac{E}{T}\right) \to \exp\!\left(-\frac{m}{T} - \frac{p^2}{2mT}\right) \ , \quad F(s) \to m_i m_j |\mathbf{v}_1 - \mathbf{v}_2| \ . \tag{D1}$$

Similarly, in (B14)

$$\gamma_3 \to \frac{m_3}{m_1 + m_2} = \frac{m_3}{m_3 + m_4} \ , \qquad \beta_3 \to 0 \ , \qquad p_3^2 \to (p'_{cm})^2 + \gamma_3^2 p_T^2 + 2p'_{cm}\gamma_3 p_T t_3 \ . \tag{D2}$$

Note that it is simpler to get the above result for p_3 from $\mathbf{p}_3 \approx \bar{\mathbf{p}}_3 + \gamma_3\mathbf{p}_T$ than from $\sqrt{E_3^2 - m_k^2}$ because there is an almost perfect cancellation in the latter.

It is further convenient to switch variables from $\mathbf{p}_1$ and $\mathbf{p}_2$ to total momentum and relative velocity

$$\mathbf{p}_T = \mathbf{p}_1 + \mathbf{p}_2 \ , \ \mathbf{v}_{rel} \equiv \mathbf{v}_1 - \mathbf{v}_2 \qquad \Leftrightarrow \qquad \mathbf{p}_1 = \frac{m_1}{m_1 + m_2}(\mathbf{p}_T + m_2\mathbf{v}_{rel}) \ , \ \mathbf{p}_2 = \frac{m_2}{m_1 + m_2}(\mathbf{p}_T - m_1\mathbf{v}_{rel}) \ , \tag{D3}$$

for which

$$d^3p_1 d^3p_2 = \left(\frac{m_1 m_2}{m_1 + m_2}\right)^3 d^3p_T d^3v_{rel} \tag{D4}$$

so

$$\int\limits_{m_i}^{\infty} dE_1 \int\limits_{m_j}^{\infty} dE_2 \int\limits_{-1}^{1} dt_{12}\, F(s)\,(...) \quad \to \quad \left(\frac{m_i m_j}{m_i + m_j}\right)^3 \int\limits_0^{\infty} dp_T \int\limits_0^{\infty} dv_{rel} \int\limits_{-1}^{1} d\cos\tilde{\theta}\ \frac{p_T^2 v_{rel}^3}{p_1 p_2}\ (...) \ , \tag{D5}$$

where $\tilde{\theta}$ is the angle between $\mathbf{p}_T$ and $\mathbf{v}_{rel}$, while in the exponents

$$\frac{p_1^2}{2m_1T} + \frac{p_2^2}{2m_2T} = \frac{p_T^2 + m_1 m_2 v_{rel}^2}{2(m_1 + m_2)T} \ . \tag{D6}$$

Straightforward integration leads then to (44).

Appendix E: Longitudinal boost invariance and Cooper-Frye integrals

For longitudinally boost invariant systems (cf. footnote [44]) hyperbolic $\eta \equiv \frac{1}{2}\ln\frac{t+z}{t-z}$ and $\tau \equiv \sqrt{t^2-z^2}$ coordinates are most convenient for spacetime, while rapidity $y \equiv \frac{1}{2}\ln\frac{E+p_z}{E-p_z}$ and transverse mass $m_T \equiv \sqrt{p_T^2+m^2}$ for momenta:

$$x^\mu = (\tau\,\mathrm{ch}\,\eta, \mathbf{x}_T, \tau\,\mathrm{sh}\,\eta) \quad , \qquad p^\mu = (m_T\,\mathrm{ch}\,y, \mathbf{p}_T, m_T\,\mathrm{sh}\,y)\ . \tag{E1}$$

The Cooper-Frye formula for the distribution of particles emitted from a surface element $d\sigma^\mu$ of a 3D spacetime hypersurface is

$$E\frac{dN_i(x,\mathbf{p})}{d^3p} \equiv \frac{dN_i(x,\mathbf{p}_T,y)}{d^2p_T dy} = p^\mu d\sigma_\mu(x) f_i(x,\mathbf{p})\ . \tag{E2}$$

Often a $\Theta(p^\mu d\sigma_\mu)$ factor is also included to cut out potential negative contributions from spacelike surface elements but it is not used in this work. With boost invariance,

$$d\sigma^\mu = n^\mu \tau d\eta d^2x_T \quad , \qquad n^\mu = (n^0\,\mathrm{ch}\,\eta, \mathbf{n}_T, n^0\,\mathrm{sh}\,\eta)\ . \tag{E3}$$

i.e.,

$$p^\mu d\sigma_\mu = \tau[m_T n^0 \mathrm{ch}\,\xi - \mathbf{p}_T\mathbf{n}_T]d\eta d^2x_T\ , \tag{E4}$$

where $\xi \equiv \eta - y$. In the thermal equilibrium distribution (4)

$$u^\mu = \gamma(\mathrm{ch}\,\eta, \mathbf{v}_T, \mathrm{sh}\,\eta) \quad , \qquad \gamma \equiv \frac{1}{\sqrt{1-v_T^2}} \qquad \Rightarrow \qquad (pu) = \gamma\,(m_T\,\mathrm{ch}\,\xi - \mathbf{p}_T\mathbf{v}_T)\ , \tag{E5}$$

and in the shear correction (23), $|\tilde{\mathbf{p}}| = \sqrt{(pu)^2-m^2}/T$,

$$\pi^{\mu\nu}p_\mu p_\nu = m_T^2(\pi^{00}\mathrm{ch}^2\xi + \pi^{zz}\mathrm{sh}^2\xi) - 2m_T\mathrm{ch}\,\xi\,(p_x\pi^{0x}+p_y\pi^{0y}) + p_x^2\pi^{xx} + p_y^2\pi^{yy} + 2p_xp_y\pi^{xy}\ , \tag{E6}$$

with shear stress components all taken at $\eta = 0$. For several equivalent forms of this expression, see Ref. [38].

Boost invariant 2+1D viscous fluid dynamics provides hydrodynamic fields (T, $\{\mu_c\}$, $\mathbf{v}_T$, $\pi^{\mu\nu}$) and hypersurface elements (n^0, $\mathbf{n}_T$) in the $\eta = 0$ frame, as a function of τ and $\mathbf{x}_T$. If one is only interested in the momentum distribution, one integrates (E2) over the hypersurface, which includes at each τ and $\mathbf{x}_T$ integration over η:

$$\tau\int_{-\infty}^{\infty} d\eta\,[m_T n^0\mathrm{ch}\,\xi - \mathbf{p}_T\mathbf{n}_T]f_i(\tau,\mathbf{x}_T,\mathbf{p}_T,\xi) = 2\tau\int_0^{\infty} d\xi\,[m_T n^0\mathrm{ch}\,\xi\eta - \mathbf{p}_T\mathbf{n}_T]f_i(\tau,\mathbf{x}_T,\mathbf{p}_T,\xi) \tag{E7}$$

with reflection symmetry along the beam axis assumed. For the ideal piece, (E7) yields

$$2\tau\frac{g_i}{(2\pi)^3}e^{\alpha_T}[m_T n^0 K_1(z_T) - \mathbf{p}_T\cdot\mathbf{n}_T K_0(z_T)] \quad , \qquad z_T \equiv \frac{\gamma m_T}{T} \quad , \qquad \alpha_T \equiv \frac{\mu_i + \gamma\mathbf{p}_T\cdot\mathbf{v}_T}{T}\ . \tag{E8}$$

For the viscous correction (23), the integral can only be evaluated analytically in special cases. For example, for quadratic corrections in momentum (34), one has[47]

$$\begin{aligned}
\frac{\chi^{Grad}}{\eta_s T^3}\frac{g_i}{(2\pi)^3}e^{\alpha_T}\ 2\tau\Bigg\{ & m_T n^0\left[m_T^2\left(K_1(z_T)+\frac{K_2(z_T)}{z_T}\right)\pi^{00} + m_T^2\frac{K_2(z_T)}{z_T}\pi^{zz} - 2m_T\left(K_0(z_T)+\frac{K_1(z_T)}{z_T}\right)\left(p_x\pi^{0x}+p_y\pi^{0y}\right)\right. \\
& \left. +\ K_1(z_T)\left(p_x^2\pi^{xx}+p_y^2\pi^{yy}+2p_xp_y\pi^{xy}\right)\right] \\
& -\mathbf{p}_T\cdot\mathbf{n}_T\left[m_T^2\left(K_0(z_T)+\frac{K_1(z_T)}{z_T}\right)\pi^{00} + m_T^2\frac{K_1(z_T)}{z_T}\pi^{zz} - 2m_T K_1(z_T)\left(p_x\pi^{0x}+p_y\pi^{0y}\right)\right. \\
& \left. +\ K_0(z_T)\left(p_x^2\pi^{xx}+p_y^2\pi^{yy}+2p_xp_y\pi^{xy}\right)\right]\Bigg\}
\end{aligned} \tag{E9}$$

Appendix F: Flow anisotropies for viscous four-source model

Here we calculate differential harmonic flow coefficients $v_n(p_T)$ for the four-source model of Sec. IV C. For isochronous emission from a spatially uniform fireball, the momentum distribution of particles is $dN/d^3p = Vf$. By assumption, the laboratory-frame volume V is the same for all four fireballs in the model. Below we construct f using viscous corrections ϕ of the Grad form (10) for each source, and then evaluate $v_n(p_T)$ via (54). It is sufficient to calculate $f_{(+x)}$ because f for the other three sources can be obtained via suitable rotation and/or mirror symmetry in the transverse plane. Unless noted otherwise, all vectors and tensors below are in laboratory (observational) frame coordinates.

For the source moving with a three-velocity $(v_x, 0, 0)$, the equilibrium phase space distribution evaluated at a general on-shell four-momentum p with azimuth such that $\mathbf{p}_T \equiv p_T(\cos\phi, \sin\phi)$ is

$$f^{\rm eq} = Ne^{-\gamma_x m_T \mathrm{ch}\, y/T} e^{\gamma_x v_x p_T \cos\phi/T} \ , \qquad N \equiv \frac{g}{(2\pi)^3} e^{\mu/T} \ , \qquad \gamma_x \equiv \frac{1}{\sqrt{1-v_x^2}} \tag{F1}$$

(cf. (4), (E1), and (E5)). The normalization N and the volume V drop out in the anisotropy coefficients. The Grad viscous corrections depend on $\pi^{\mu\nu}p_\mu p_\nu$ given by (E6). Instead of boosting (41) to obtain the shear stress tensor for the fireball, it is simpler to evaluate this scalar via inverse boosting p to the fluid rest frame, where

$$p^\mu_{LR} = (\gamma_x(m_T \mathrm{ch}\, y - v_x p_T \cos\phi), \gamma_x(p_T\cos\phi - v_x m_T \mathrm{ch}\, y), p_T \sin\phi, m_T \mathrm{sh}\, y) \ , \tag{F2}$$

and $\pi^{\mu\nu}_{LR}$ is diagonal. Straightforward algebra then yields, at midrapidity $y = 0$,

$$f_{(+x)} = Ne^{-a_x} e^{b_x\cos\phi}\left[1 + \frac{c\kappa}{4}(z^2 - a_x^2 + 2a_x b_x \cos\phi - b_x^2\cos^2\phi)\right] \tag{F3}$$

with

$$\kappa \equiv \frac{\pi_L}{e+p} \ , \qquad z \equiv \frac{m}{T} \ , \tag{F4}$$

and shorthands

$$a_x \equiv \frac{\gamma_x m_T}{T} \ , \qquad b_x \equiv \frac{\gamma_x v_x p_T}{T} \ . \tag{F5}$$

Species dependence enters through the mass in z and a_x, and for dynamical Grad corrections also through c. For the democratic Grad ansatz, only the mass matters because $c = 1$ is set for all species.

Ninety-degree rotation $\phi \to \phi - \pi/2$ and substitution $v_x \to v_y$ gives $f_{(+y)}$, and similar rotations by π and $3\pi/2$, or equivalently, reflections $v_x \to -v_x$, $v_y \to -v_y$, give the remaining two source distributions. Thus, at midrapidity,

$$f(p_T,\phi) = f_{(+x)} + f_{(+x)}\big|_{b_x\to -b_x} + f_{(+x)}\big|^{a_x\to a_y}_{\substack{b_x\to b_y \\ \cos\phi\to\sin\phi}} + f_{(+x)}\big|^{a_x\to a_y}_{\substack{b_x\to -b_y \\ \cos\phi\to\sin\phi}} \ . \tag{F6}$$

Harmonic flow coefficients (54) can now be readily evaluated. Each term in the denominator reduces to the integral over $f_{(+x)}$ via shifts $\phi \to \phi - \pi/2$, $\phi \to \phi - \pi$, $\phi \to \phi - 3\pi/2$ in the integrals for $f_{(+y)}$, $f_{(-x)}$, $f_{(-y)}$, respectively, which do not affect the range of integration. Analogous shifts of ϕ in the numerator have the potential side effect of changing the sign of $\cos(n\phi)$. For odd n, a shift by π brings a minus sign and, therefore, contributions cancel, i.e., $v_n = 0$ (this is also evident from the symmetry of the configuration). For even n, a shift by π preserves the sign, so the sources moving along the $\pm x$ directions contribute equally. Shifts by $\pi/2$ and $3\pi/2$ flip sign in the numerator whenever n is not divisible by 4, so the sources moving along the $\pm y$ direction also contribute equally but with potentially opposite overall sign. Therefore, for even n,

$$v_n(p_T) = \frac{G_n(a_x, b_x, z, c\kappa) + (-1)^{n/2} G_n(a_y, b_y, z, c\kappa)}{G_0(a_x, b_x, z, c\kappa) + G_0(a_y, b_y, z, c\kappa)} \ , \tag{F7}$$

where the shorthand

$$\begin{aligned} G_n(a_x, b_x, z, c\kappa) \ &\equiv \ \frac{1}{2\pi N}\int_0^{2\pi} d\phi\, f_{(+x)}\, \cos(n\phi) \\ &= \ e^{-a_x}\left\{ I_n + \frac{c\kappa}{4}\left[(z^2 - a_x^2) I_n + a_x b_x (I_{|n-1|} + I_{n+1}) - \frac{b_x^2}{4}(I_{|n-2|} + 2I_n + I_{n+2})\right]\right\} \end{aligned} \tag{F8}$$

involves modified Bessel functions of the first kind

$$I_n \equiv I_n(b_x) \equiv \frac{1}{2\pi}\int_0^{2\pi} d\varphi\, e^{b_x\cos\varphi}\cos(n\varphi)\ . \tag{F9}$$

(Integrals with $\cos\phi\cos(n\phi)$ and $\cos^2\phi\cos(n\phi)$ reduce to those with a single cosine with the help of the cosine addition theorem and $\cos^2\phi \equiv (\cos 2\phi + 1)/2$.) Note that for $\kappa \leq 0$ the denominator in (F7) is strictly positive because, at midrapidity, $\pi^{\mu\nu}p_\mu p_\nu = -\pi_L(p_{x,LR}^2 + p_{y,LR}^2)/2 \geq 0$.

Appendix G: Self-consistent Grad coefficient tables

Tables V-VI, VII-VIII, and IX-X tabulate self-consistent viscous phase space corrections for the gas of hadrons in Section V, using $\delta f/f^{\rm eq} \propto p^2$, $p^{3/2}$ and p, respectively. In all six tables, correction factors *relative* to the "democratic Grad" form (10) are printed (rounded to two decimal figures). To apply the dynamical correction for species i, read the coefficient c_i from the table for the species and multiply democratic viscous corrections by the expression in (58) that corresponds to the desired momentum dependence.

The corrections depend rather smoothly on hadron (pole) mass, and therefore can also be well represented by fits of the form

$$c(x) = \delta + \alpha\left[1 + \left(\frac{x}{\gamma}\right)^\beta\right]^{-1} \qquad \text{or} \qquad c(x) = \alpha + \beta|x-\gamma|^\delta\ , \qquad x \equiv \frac{m}{1\ \text{GeV}}\ , \tag{G1}$$

where x is the hadron (pole) mass m in GeV units. Tables XI-XIII list the best fit values for the parameters α, β, γ, and δ as a function of temperature for the various scenarios in Tables V-X. The fits are done to the original unrounded c_i values. Note that there are separate fits for mesons and baryons in the case of additive quark model (AQM) cross sections. There is no specific physics motivation behind the forms (G1); the functions are chosen solely for accuracy (the relative accuracy is better than 8.5×10^{-4} in all cases).

TABLE V: Species-dependent shear viscous phase space corrections calculated as a function of temperature for a gas of hadrons up to $m = 1.672$ GeV with the same constant cross section for all species, assuming quadratic momentum dependence $\delta f/f^{eq} \propto p^2$ (dynamical Grad approximation).

Species	T = 100	120	140	165 MeV
π	1.08	1.13	1.17	1.21
K	0.89	0.96	1.02	1.08
η	0.87	0.94	1.00	1.06
f_0	0.85	0.92	0.98	1.04
ρ	0.80	0.87	0.93	0.99
ω	0.80	0.86	0.93	0.99
$K^*(892)$	0.77	0.83	0.90	0.96
N	0.76	0.82	0.88	0.94
$\eta'(958)$	0.75	0.82	0.88	0.94
$f_0(980)$	0.75	0.81	0.87	0.93
$a_0(980)$	0.75	0.81	0.87	0.93
$\phi(1020)$	0.74	0.81	0.86	0.92
Λ	0.72	0.79	0.84	0.90
$h_1(1170)$	0.72	0.78	0.83	0.89
Σ	0.71	0.77	0.83	0.89
$b_1(1235)$	0.71	0.76	0.82	0.88
$\Delta(1232)$	0.71	0.76	0.82	0.88
$a_1(1260)$	0.71	0.77	0.82	0.88
$K_1(1270)$	0.70	0.76	0.81	0.87
$f_2(1270)$	0.70	0.76	0.81	0.87
$f_1(1285)$	0.70	0.76	0.81	0.87
$\eta(1295)$	0.70	0.75	0.81	0.87
$\pi(1300)$	0.70	0.75	0.81	0.87
Ξ	0.69	0.75	0.81	0.86
$a_2(1320)$	0.69	0.75	0.81	0.86
$\Sigma(1385)$	0.68	0.74	0.80	0.85
$f_0(1370)$	0.69	0.74	0.80	0.85
$K_1(1400)$	0.68	0.74	0.79	0.85
$\Lambda(1405)$	0.68	0.74	0.79	0.85
$K^*(1410)$	0.68	0.74	0.79	0.85
$\eta(1405)$	0.68	0.74	0.79	0.85
$\omega(1420)$	0.68	0.74	0.79	0.84
$f_1(1420)$	0.68	0.73	0.79	0.84
$K_0^*(1430)$	0.68	0.73	0.79	0.84
$K_2^*(1430)$	0.68	0.73	0.79	0.84
N(1440)	0.68	0.73	0.79	0.84
$\rho(1450)$	0.67	0.73	0.78	0.84
$f_0(1500)$	0.67	0.72	0.78	0.83
$\Lambda(1520)$	0.67	0.72	0.77	0.83
N(1520)	0.67	0.72	0.77	0.83
$f_2'(1525)$	0.67	0.72	0.77	0.83
$\Xi(1530)$	0.67	0.72	0.77	0.83
N(1535)	0.67	0.72	0.77	0.83
$\Delta(1600)$	0.66	0.71	0.76	0.82
$\Lambda(1600)$	0.66	0.71	0.76	0.82
$\Delta(1620)$	0.66	0.71	0.76	0.81
$\omega(1650)$	0.65	0.71	0.76	0.81
N(1650)	0.65	0.71	0.76	0.81
Ω	0.65	0.70	0.75	0.81

TABLE VI: Species-dependent shear viscous phase space corrections calculated as a function of temperature for a gas of hadrons up to $m = 1.672$ GeV with additive quark model[31] (AQM) cross sections, assuming quadratic momentum dependence $\delta f/f^{eq} \propto p^2$ (dynamical Grad approximation).

Species	T = 100	120	140	165 MeV
π	1.08	1.15	1.21	1.27
K	0.90	0.98	1.06	1.14
η	0.88	0.95	1.03	1.12
f_0	0.86	0.94	1.01	1.10
ρ	0.80	0.88	0.96	1.04
ω	0.80	0.88	0.95	1.04
$K^*(892)$	0.77	0.85	0.92	1.01
N	0.56	0.62	0.68	0.74
$\eta'(958)$	0.76	0.83	0.91	0.99
$f_0(980)$	0.75	0.83	0.90	0.98
$a_0(980)$	0.75	0.83	0.90	0.98
$\phi(1020)$	0.75	0.82	0.89	0.97
Λ	0.53	0.59	0.64	0.70
$h_1(1170)$	0.72	0.79	0.86	0.94
Σ	0.52	0.58	0.63	0.69
$b_1(1235)$	0.71	0.78	0.85	0.93
$\Delta(1232)$	0.52	0.57	0.62	0.68
$a_1(1260)$	0.71	0.78	0.85	0.93
$K_1(1270)$	0.70	0.77	0.84	0.92
$f_2(1270)$	0.70	0.77	0.84	0.92
$f_1(1285)$	0.70	0.77	0.84	0.92
$\eta(1295)$	0.70	0.77	0.84	0.91
$\pi(1300)$	0.70	0.77	0.83	0.91
Ξ	0.51	0.56	0.61	0.67
$a_2(1320)$	0.70	0.76	0.83	0.91
$\Sigma(1385)$	0.50	0.55	0.60	0.66
$f_0(1370)$	0.69	0.75	0.82	0.90
$K_1(1400)$	0.68	0.75	0.82	0.89
$\Lambda(1405)$	0.50	0.55	0.60	0.66
$K^*(1410)$	0.68	0.75	0.82	0.89
$\eta(1405)$	0.68	0.75	0.82	0.89
$\omega(1420)$	0.68	0.75	0.81	0.89
$f_1(1420)$	0.68	0.75	0.81	0.89
$K_0^*(1430)$	0.68	0.75	0.81	0.89
$K_2^*(1430)$	0.68	0.75	0.81	0.89
N(1440)	0.49	0.54	0.60	0.65
$\rho(1450)$	0.68	0.74	0.81	0.88
$f_0(1500)$	0.67	0.74	0.80	0.88
$\Lambda(1520)$	0.48	0.53	0.59	0.64
N(1520)	0.48	0.53	0.59	0.64
$f_2'(1525)$	0.67	0.73	0.80	0.87
$\Xi(1530)$	0.48	0.53	0.58	0.64
N(1535)	0.48	0.53	0.58	0.64
$\Delta(1600)$	0.48	0.53	0.58	0.63
$\Lambda(1600)$	0.48	0.53	0.58	0.63
$\Delta(1620)$	0.48	0.52	0.57	0.63
$\omega(1650)$	0.66	0.72	0.78	0.85
N(1650)	0.47	0.52	0.57	0.63
Ω	0.47	0.52	0.57	0.62

TABLE VII: Species-dependent shear viscous phase space corrections calculated as a function of temperature for a gas of hadrons up to $m = 1.672$ GeV with the same constant cross section for all species, assuming power-law momentum dependence $\delta f/f^{eq} \propto p^{3/2}$.

Species	T = 100	120	140	165 MeV
π	2.56	2.68	2.79	2.87
K	2.31	2.45	2.58	2.69
η	2.28	2.42	2.55	2.66
f_0	2.26	2.39	2.52	2.64
ρ	2.19	2.32	2.45	2.57
ω	2.19	2.32	2.44	2.56
$K^*(892)$	2.15	2.28	2.41	2.52
N	2.14	2.27	2.39	2.51
$\eta'(958)$	2.14	2.26	2.38	2.50
$f_0(980)$	2.13	2.26	2.38	2.49
$a_0(980)$	2.13	2.25	2.38	2.49
$\phi(1020)$	2.12	2.24	2.37	2.48
Λ	2.10	2.22	2.34	2.45
$h_1(1170)$	2.09	2.21	2.32	2.44
Σ	2.09	2.20	2.32	2.43
$b_1(1235)$	2.08	2.20	2.31	2.42
$\Delta(1232)$	2.08	2.20	2.31	2.42
$a_1(1260)$	2.08	2.20	2.31	2.42
$K_1(1270)$	2.07	2.19	2.30	2.41
$f_2(1270)$	2.07	2.19	2.30	2.41
$f_1(1285)$	2.07	2.19	2.30	2.41
$\eta(1295)$	2.07	2.18	2.30	2.40
$\pi(1300)$	2.07	2.18	2.29	2.40
Ξ	2.07	2.18	2.29	2.40
$a_2(1320)$	2.07	2.18	2.29	2.40
$\Sigma(1385)$	2.06	2.17	2.28	2.38
$f_0(1370)$	2.06	2.17	2.28	2.39
$K_1(1400)$	2.06	2.17	2.27	2.38
$\Lambda(1405)$	2.06	2.16	2.27	2.38
$K^*(1410)$	2.06	2.16	2.27	2.38
$\eta(1405)$	2.06	2.16	2.27	2.38
$\omega(1420)$	2.05	2.16	2.27	2.38
$f_1(1420)$	2.05	2.16	2.27	2.37
$K_0^*(1430)$	2.05	2.16	2.27	2.37
$K_2^*(1430)$	2.05	2.16	2.27	2.37
N(1440)	2.05	2.16	2.27	2.37
$\rho(1450)$	2.05	2.16	2.26	2.37
$f_0(1500)$	2.04	2.15	2.26	2.36
$\Lambda(1520)$	2.04	2.15	2.25	2.35
N(1520)	2.04	2.15	2.25	2.35
$f_2'(1525)$	2.04	2.15	2.25	2.35
$\Xi(1530)$	2.04	2.15	2.25	2.35
N(1535)	2.04	2.15	2.25	2.35
$\Delta(1600)$	2.03	2.14	2.24	2.34
$\Lambda(1600)$	2.03	2.14	2.24	2.34
$\Delta(1620)$	2.03	2.13	2.24	2.34
$\omega(1650)$	2.03	2.13	2.23	2.33
N(1650)	2.03	2.13	2.23	2.33
Ω	2.03	2.13	2.23	2.33

TABLE VIII: Species-dependent shear viscous phase space corrections calculated as a function of temperature for a gas of hadrons up to $m = 1.672$ GeV with additive quark model[31] (AQM) cross sections, assuming power-law momentum dependence $\delta f/f^{eq} \propto p^{3/2}$.

Species	T = 100	120	140	165 MeV
π	2.57	2.72	2.87	3.03
K	2.32	2.48	2.66	2.83
η	2.29	2.45	2.63	2.81
f_0	2.27	2.43	2.60	2.78
ρ	2.20	2.36	2.52	2.70
ω	2.20	2.35	2.52	2.70
$K^*(892)$	2.16	2.31	2.48	2.66
N	1.57	1.69	1.81	1.95
$\eta'(958)$	2.15	2.30	2.46	2.63
$f_0(980)$	2.14	2.29	2.45	2.63
$a_0(980)$	2.14	2.29	2.45	2.62
$\phi(1020)$	2.13	2.28	2.44	2.61
Λ	1.53	1.65	1.77	1.90
$h_1(1170)$	2.10	2.24	2.40	2.57
Σ	1.52	1.63	1.75	1.88
$b_1(1235)$	2.09	2.23	2.38	2.55
$\Delta(1232)$	1.51	1.62	1.74	1.87
$a_1(1260)$	2.09	2.23	2.38	2.55
$K_1(1270)$	2.08	2.22	2.37	2.54
$f_2(1270)$	2.08	2.22	2.37	2.54
$f_1(1285)$	2.08	2.22	2.37	2.54
$\eta(1295)$	2.08	2.22	2.37	2.53
$\pi(1300)$	2.08	2.22	2.37	2.53
Ξ	1.50	1.61	1.73	1.85
$a_2(1320)$	2.08	2.21	2.36	2.53
$\Sigma(1385)$	1.49	1.60	1.71	1.84
$f_0(1370)$	2.07	2.20	2.35	2.52
$K_1(1400)$	2.07	2.20	2.34	2.51
$\Lambda(1405)$	1.49	1.59	1.71	1.83
$K^*(1410)$	2.06	2.20	2.34	2.51
$\eta(1405)$	2.06	2.19	2.34	2.50
$\omega(1420)$	2.06	2.19	2.34	2.50
$f_1(1420)$	2.06	2.19	2.34	2.50
$K_0^*(1430)$	2.06	2.19	2.34	2.50
$K_2^*(1430)$	2.06	2.19	2.34	2.50
N(1440)	1.49	1.59	1.70	1.83
$\rho(1450)$	2.06	2.19	2.33	2.49
$f_0(1500)$	2.05	2.18	2.33	2.49
$\Lambda(1520)$	1.48	1.58	1.69	1.81
N(1520)	1.48	1.58	1.69	1.81
$f_2'(1525)$	2.05	2.18	2.32	2.48
$\Xi(1530)$	1.48	1.58	1.69	1.81
N(1535)	1.47	1.58	1.69	1.81
$\Delta(1600)$	1.47	1.57	1.68	1.80
$\Lambda(1600)$	1.47	1.57	1.68	1.80
$\Delta(1620)$	1.47	1.57	1.68	1.80
$\omega(1650)$	2.04	2.16	2.30	2.46
N(1650)	1.46	1.56	1.67	1.79
Ω	1.46	1.56	1.67	1.79

TABLE IX: Species-dependent shear viscous phase space corrections calculated as a function of temperature for a gas of hadrons up to $m = 1.672$ GeV with the same constant cross section for all species, assuming linear momentum dependence $\delta f/f^{eq} \propto p$.

Species	T = 100	120	140	165 MeV
π	5.81	6.06	6.29	6.49
K	5.78	6.03	6.27	6.46
η	5.79	6.03	6.27	6.46
f_0	5.79	6.03	6.27	6.46
ρ	5.82	6.04	6.27	6.46
ω	5.82	6.04	6.27	6.46
$K^*(892)$	5.85	6.06	6.28	6.46
N	5.86	6.07	6.28	6.46
$\eta'(958)$	5.87	6.07	6.28	6.46
$f_0(980)$	5.87	6.07	6.29	6.46
$a_0(980)$	5.87	6.07	6.29	6.46
$\phi(1020)$	5.88	6.08	6.29	6.46
Λ	5.91	6.10	6.30	6.47
$h_1(1170)$	5.93	6.11	6.31	6.47
Σ	5.94	6.11	6.31	6.47
$b_1(1235)$	5.95	6.12	6.32	6.48
$\Delta(1232)$	5.95	6.12	6.32	6.48
$a_1(1260)$	5.95	6.12	6.32	6.48
$K_1(1270)$	5.96	6.13	6.32	6.48
$f_2(1270)$	5.96	6.13	6.32	6.48
$f_1(1285)$	5.97	6.14	6.32	6.48
$\eta(1295)$	5.97	6.14	6.33	6.48
$\pi(1300)$	5.97	6.14	6.33	6.48
Ξ	5.98	6.14	6.33	6.48
$a_2(1320)$	5.98	6.14	6.33	6.48
$\Sigma(1385)$	6.00	6.16	6.34	6.49
$f_0(1370)$	6.00	6.16	6.34	6.49
$K_1(1400)$	6.01	6.16	6.34	6.49
$\Lambda(1405)$	6.01	6.17	6.34	6.49
$K^*(1410)$	6.01	6.17	6.34	6.49
$\eta(1405)$	6.01	6.17	6.34	6.49
$\omega(1420)$	6.02	6.17	6.35	6.49
$f_1(1420)$	6.02	6.17	6.35	6.49
$K_0^*(1430)$	6.02	6.17	6.35	6.49
$K_2^*(1430)$	6.02	6.17	6.35	6.49
N(1440)	6.02	6.17	6.35	6.49
$\rho(1450)$	6.03	6.18	6.35	6.50
$f_0(1500)$	6.05	6.19	6.36	6.50
$\Lambda(1520)$	6.05	6.19	6.36	6.50
N(1520)	6.05	6.20	6.36	6.50
$f_2'(1525)$	6.05	6.20	6.36	6.50
$\Xi(1530)$	6.06	6.20	6.37	6.50
N(1535)	6.06	6.20	6.37	6.50
$\Delta(1600)$	6.08	6.22	6.38	6.51
$\Lambda(1600)$	6.08	6.22	6.38	6.51
$\Delta(1620)$	6.09	6.22	6.38	6.51
$\omega(1650)$	6.10	6.23	6.39	6.52
N(1650)	6.10	6.23	6.39	6.52
Ω	6.11	6.24	6.39	6.52

TABLE X: Species-dependent shear viscous phase space corrections calculated as a function of temperature for a gas of hadrons up to $m = 1.672$ GeV with additive quark model[31] (AQM) cross sections, assuming linear momentum dependence $\delta f/f^{eq} \propto p$.

Species	T = 100	120	140	165 MeV
π	5.84	6.15	6.49	6.84
K	5.81	6.12	6.46	6.81
η	5.81	6.12	6.46	6.81
f_0	5.82	6.12	6.46	6.81
ρ	5.85	6.13	6.46	6.81
ω	5.85	6.13	6.46	6.81
$K^*(892)$	5.88	6.15	6.47	6.81
N	4.25	4.47	4.72	4.97
$\eta'(958)$	5.89	6.16	6.48	6.81
$f_0(980)$	5.90	6.16	6.48	6.81
$a_0(980)$	5.90	6.16	6.48	6.81
$\phi(1020)$	5.91	6.17	6.48	6.82
Λ	4.27	4.47	4.72	4.96
$h_1(1170)$	5.96	6.20	6.50	6.82
Σ	4.28	4.48	4.72	4.96
$b_1(1235)$	5.98	6.21	6.51	6.83
$\Delta(1232)$	4.29	4.48	4.72	4.96
$a_1(1260)$	5.98	6.21	6.51	6.83
$K_1(1270)$	5.99	6.22	6.52	6.83
$f_2(1270)$	5.99	6.22	6.52	6.83
$f_1(1285)$	5.99	6.23	6.52	6.83
$\eta(1295)$	6.00	6.23	6.52	6.83
$\pi(1300)$	6.00	6.23	6.52	6.83
Ξ	4.30	4.49	4.72	4.96
$a_2(1320)$	6.01	6.23	6.52	6.84
$\Sigma(1385)$	4.31	4.50	4.72	4.96
$f_0(1370)$	6.02	6.25	6.53	6.84
$K_1(1400)$	6.04	6.25	6.54	6.84
$\Lambda(1405)$	4.31	4.50	4.73	4.96
$K^*(1410)$	6.04	6.26	6.54	6.85
$\eta(1405)$	6.04	6.26	6.54	6.85
$\omega(1420)$	6.04	6.26	6.54	6.85
$f_1(1420)$	6.05	6.26	6.54	6.85
$K_0^*(1430)$	6.05	6.26	6.54	6.85
$K_2^*(1430)$	6.04	6.26	6.54	6.85
N(1440)	4.32	4.50	4.73	4.96
$\rho(1450)$	6.06	6.27	6.55	6.85
$f_0(1500)$	6.07	6.28	6.56	6.86
$\Lambda(1520)$	4.33	4.51	4.73	4.97
N(1520)	4.33	4.51	4.73	4.97
$f_2'(1525)$	6.08	6.29	6.56	6.86
$\Xi(1530)$	4.34	4.51	4.73	4.97
N(1535)	4.34	4.51	4.73	4.97
$\Delta(1600)$	4.35	4.52	4.74	4.97
$\Lambda(1600)$	4.35	4.52	4.74	4.97
$\Delta(1620)$	4.35	4.52	4.74	4.97
$\omega(1650)$	6.13	6.32	6.59	6.87
N(1650)	4.36	4.53	4.74	4.97
Ω	4.36	4.53	4.74	4.97

TABLE XI: Parameters as a function of temperature for the fit function $c(x) = \delta + \alpha/[1 + (x/\gamma)^{\beta}]$ to the species-dependent Grad shear viscous phase space corrections listed in Tables V-VI.

$\sigma = const$ scenario (Grad)				
T [MeV]	α	β	γ	δ
100	0.698	1.204	0.715	0.467
120	0.700	1.266	0.862	0.493
140	0.702	1.326	0.996	0.519
165	0.693	1.397	1.140	1.243
AQM scenario, mesons (Grad)				
T [MeV]	α	β	γ	δ
100	0.696	1.214	0.712	0.472
120	0.704	1.278	0.856	0.505
140	0.715	1.342	0.985	0.543
165	0.717	1.414	1.124	0.591
AQM scenario, baryons (Grad)				
T [MeV]	α	β	γ	δ
100	0.687	1.009	0.623	0.286
120	0.698	1.037	0.801	0.297
140	0.710	1.075	0.987	0.311
165	0.711	1.129	1.204	0.334

TABLE XII: Parameters as a function of temperature for the fit function $c(x) = \delta + \alpha/[1 + (x/\gamma)^{\beta}]$ to the species-dependent $p^{3/2}$ shear viscous phase space corrections listed in Tables VII-VIII.

$\sigma = const$ scenario ($p^{3/2}$)				
T [MeV]	α	β	γ	δ
100	0.748	1.446	0.559	1.900
120	0.823	1.375	0.712	1.933
140	0.883	1.363	0.876	1.969
165	0.921	1.386	1.061	2.006
AQM scenario, mesons ($p^{3/2}$)				
T [MeV]	α	β	γ	δ
100	0.759	1.427	0.561	1.904
120	0.839	1.370	0.714	1.959
140	0.908	1.367	0.874	2.032
165	0.957	1.397	1.047	2.126
AQM scenario, baryons ($p^{3/2}$)				
T [MeV]	α	β	γ	δ
100	0.540	1.627	0.760	1.344
120	0.691	1.396	0.836	1.369
140	0.806	1.288	0.974	1.400
165	0.890	1.243	1.177	1.439

TABLE XIII: Parameters as a function of temperature for the fit function $c(x) = \alpha + \beta|x - \gamma|^{\delta}$ to the species-dependent p^1 shear viscous phase space corrections listed in Tables IX-X.

$\sigma = const$ scenario (p^1)				
T [MeV]	α	β	γ	δ
100	5.775	0.240	0.419	1.521
120	6.025	0.166	0.502	1.633
140	6.265	0.114	0.599	1.734
165	6.458	0.073	0.747	1.882
AQM scenario, mesons (p^1)				
T [MeV]	α	β	γ	δ
100	5.802	0.239	0.419	1.546
120	6.114	0.167	0.504	1.655
140	6.459	0.118	0.603	1.743
165	6.808	0.080	0.742	1.865
AQM scenario, baryons (p^1)				
T [MeV]	α	β	γ	δ
100	4.245	0.156	0.848	1.404
120	4.466	0.097	0.897	1.603
140	4.715	0.062	1.015	1.842
165	4.963	0.045	1.293	1.931

[1] For reviews, see, e.g., P. Huovinen and P. V. Ruuskanen, Ann. Rev. Nucl. Part. Sci. **56**, 163 (2006); D. A. Teaney, arXiv:0905.2433 [nucl-th]; or C. Gale, S. Jeon and B. Schenke, Int. J. Mod. Phys. A **28**, 1340011 (2013).
[2] P. Huovinen and H. Petersen, Eur. Phys. J. A **48**, 171 (2012).
[3] F. Cooper and G. Frye, Phys. Rev. D **10**, 186 (1974).
[4] H. Song, S. A. Bass, U. Heinz, T. Hirano and C. Shen, Phys. Rev. C **83**, 054910 (2011) [Erratum-ibid. C **86**, 059903 (2012)].
[5] D. Molnar, J. Phys. G **38**, 124173 (2011).
[6] K. Dusling, G. D. Moore and D. Teaney, Phys. Rev. C **81**, 034907 (2010).
[7] A. Monnai and T. Hirano, Phys. Rev. C **80**, 054906 (2009).
[8] K. Dusling and T. Schäfer, Phys. Rev. C **85**, 044909 (2012).
[9] J. Noronha-Hostler, G. S. Denicol, J. Noronha, R. P. G. Andrade and F. Grassi, Phys. Rev. C **88**, 044916 (2013).
[10] B. Schenke and M. Strickland, Phys. Rev. D **76**, 025023 (2007).
[11] For an alternative approach that considers a rapid conversion *process* in a thin layer idealized as hypersurface in spacetime, with the process constrained by energy-momentum and current conservation across the hypersurface, and the nondecrease of entropy, see C. Anderlik, Z. I. Lazar, V. K. Magas, L. P. Csernai, H. Stoecker and W. Greiner, Phys. Rev. C **59**, 388 (1999); and V. K. Magas, A. Anderlik, C. Anderlik and L. P. Csernai, Eur. Phys. J. C **30**, 255 (2003).
[12] G. S. Denicol, H. Niemi, E. Molnar and D. H. Rischke, Phys. Rev. D **85**, 114047 (2012) [Phys. Rev. D **91**, no. 3, 039902 (2015)].
[13] See, e.g., Chapter VI of Ref. [14], or for a more recent presentation Section 3 of Ref. [15].
[14] S. R. de Groot, W. A. van Leeuwen, Ch. G. van Weert, *Relativistic kinetic theory - Principles and applications* (North-Holland, 1980).
[15] P. B. Arnold, G. D. Moore and L. G. Yaffe, JHEP **0011**, 001 (2000).
[16] P. Huovinen and D. Molnar, Phys. Rev. C **79**, 014906 (2009).
[17] D. Molnar and M. Gyulassy, Phys. Rev. C **62**, 054907 (2000).
[18] D. Molnar, MPC 1.8.13. This transport code is available at http://karman.physics.purdue.edu/OSCAR
[19] A. El, I. Bouras, C. Wesp, Z. Xu and C. Greiner, Eur. Phys. J. A **48**, 166 (2012).
[20] M. Prakash, M. Prakash, R. Venugopalan and G. Welke, Phys. Rept. **227**, 321 (1993).
[21] P. F. Kolb, J. Sollfrank and U. W. Heinz, Phys. Rev. C **62**, 054909 (2000); P. F. Kolb and R. Rapp, Phys. Rev. C **67**, 044903 (2003); P. F. Kolb and U. W. Heinz, In *Hwa, R.C. (ed.) et al.: Quark gluon plasma* 634-714 [nucl-th/0305084].
[22] The original version 0.2 of AZHYDRO and version 0.2p2 patched by P. Huovinen and D. Molnar are available on the WWW from the Open Standard Codes and Routines (OSCAR) repository at http://karman.physics.purdue.edu/OSCAR
[23] P. Huovinen and P. Petreczky, Nucl. Phys. A **837**, 26 (2010).
[24] D. Teaney, Phys. Rev. C **68**, 034913 (2003).
[25] K Dusling and D Teaney, Phys. Rev. C **77**, 034905 (2008).
[26] D. Molnar and P. Huovinen, J. Phys. G **35**, 104125 (2008).
[27] M. Bleicher, E. Zabrodin, C. Spieles, S. A. Bass, C. Ernst, S. Soff, L. Bravina, M. Belkacem, H. Weber, H. Stöcker, and W. Greiner, J. Phys. G **G25**, 1859 (1999); H. Petersen, M. Bleicher, S. A. Bass and H. Stocker, arXiv:0805.0567 [hep-ph].
[28] Z. W. Lin, C. M. Ko, B. A. Li, B. Zhang and S. Pal, Phys. Rev. C **72**, 064901 (2005).
[29] Y. Nara, N. Otuka, A. Ohnishi, K. Niita and S. Chiba, Phys. Rev. C **61**, 024901 (2000).
[30] G. S. Denicol and H. Niemi, Nucl. Phys. A **904-905**, 369c (2013).
[31] E. M. Levin and L. L. Frankfurt, JETP Lett. **2**, 65 (1965); V. V. Anisovich, M. N. Kobrinsky, J. Nyiri and Y. .M. Shabelski, Sov. Phys. Usp. **27**, 901 (1984) [Usp. Fiz. Nauk **144**, 553 (1984)].
[32] P. Huovinen, P. F. Kolb, U. W. Heinz, P. V. Ruuskanen and S. A. Voloshin, Phys. Lett. B **503**, 58 (2001).
[33] For properties of irreducible tensors, see Section VI.2a of Ref. [14], or Appendix F of Ref. [12].
[34] GNU Scientific Library (GSL) version 1.14. Source code and documentation are available from the GNU website at http://www.gnu.org/s/gsl
[35] B. Zhang, M. Gyulassy and Y. Pang, Phys. Rev. C **58**, 1175 (1998).
[36] B. Tomasik and U. A. Wiedemann, Phys. Rev. C **68**, 034905 (2003).
[37] P. Huovinen, talk at 2nd International Symposium on Nonequilibrium Dynamics and 3rd Network Workshop on Theory of Ultrarelativistic Heavy Ion Collisions (NeD/TURIC-2012), June 25-30, 2012. Slides can be downloaded from the WWW at http://fias.uni-frankfurt.de/crete2012/talks/30/Huovinen.pdf
[38] H. Song and U. W. Heinz, Phys. Rev. C **77**, 064901 (2008).
[39] High-energy physics units $\hbar = c = k_B = 1$ and the metric with $(+,-,-,-)$ signature are used throughout, with Einstein conventions in all Lorentz tensor expressions, and Minkowski scalar products abbreviated as $(ab) \equiv a_\mu b^\mu$. Sums over particle species, on the other hand, are always written explicitly.
[40] Throughout this paper Boltzmann statistics is assumed but generalization to the Bose/Fermi case is straightforward.
[41] In (13) outgoing momenta p_3 and p_4 are understood to be integrated over full, unrestricted phasespace. This double-counts the rate for identical particles ($k = \ell$) compared to nonidentical particles, however, that is compensated by double-counting in the sum for $k \neq \ell$. See also (B3).
[42] δf_i is to leading order proportional to the gradients of $f_i^{\rm eq}$, and if those are small due to a large length scale L in the problem $\nabla_\mu f_i^{\rm eq} \sim 1/L$, then $\nabla_\mu \delta f_i \sim 1/L^2$ is suppressed compared to $\nabla_\mu f_i$.

[43] Time derivatives of hydrodynamic quantities can be replaced with spatial ones using the energy-momentum and charge conservation laws $\partial_\mu T^{\mu\nu}(x) = 0$, $\partial_\mu N_c^\mu(x) = 0$. For example,

$$(u\partial)u^\nu = \frac{1}{e+p}[\nabla^\nu p - \nabla_\mu \delta T^{\mu\nu} + \delta T^{\mu\nu}(u\partial)u_\mu] \ , \quad (u\partial)n_c = -n_c(\nabla u) - \nabla_\mu \delta N_c^\mu + \delta N_c^\mu (u\partial)u_\mu \ ,$$

and note that $(\partial u) \equiv (\nabla u)$. In shear viscosity calculations, pressure, energy density, and charge densities are uniform by assumption, so derivatives of those vanish as well as derivatives of T and μ_c. What remains are first derivatives of dissipative corrections, and dissipative corrections times first derivatives of ideal hydrodynamic fields. In the Navier-Stokes regime these are of the same order and correspond to second derivatives of the ideal fields.

[44] By longitudinal boost invariance we mean that the state of the system at each point in spacetime with $t > 0$, coordinate rapidity $\eta \neq 0$ can be obtained from the state on the $\eta = 0$ sheet via Lorentz boost along the z direction.

[45] In a scale invariant system all cross sections are set by the temperature, i.e., $\sigma \propto 1/T^2$. However, as shown in Ref. [16], $\sigma \propto 1/T^2$ is very well approximated by $\sigma \propto \tau^{2/3}$ because for 0+1D Bjorken expansion $T \propto \tau^{-1/3}$ as long as the system is near local equilibrium.

[46] We trust that the reader will not confuse the momentum rapidity variable y and the y axis in the transverse plane.

[47] There are many equivalent ways to write these expressions because of Bessel function identities, such as $K_{n-1}(x) + 2nK_n(x)/x \equiv K_{n+1}(x)$.